Data-Driven Materials Discovery and Synthesis using Machine Learning Methods

Sterling G. Baird[a], Marianne Liu[a,b], Hasan M. Sayeed[a], Taylor D. Sparks[a,*]

[a] *Department of Materials Science and Engineering, University of Utah, Salt Lake City, Utah 84112, USA*
[b] *West High School, Salt Lake City, Utah 84112, USA*

arXiv:2202.02380v1 [cond-mat.mtrl-sci] 25 Jan 2022

Abstract

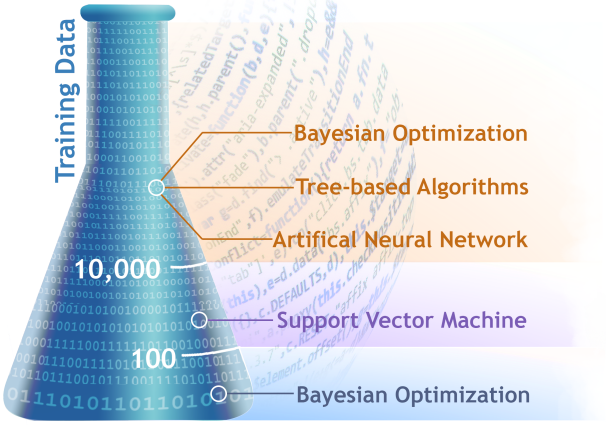

Experimentally [1–38] and computationally [39–50] validated machine learning (ML) articles are sorted based on size of the training data: 1–100, 101–10 000, and 10 000+ in a comprehensive set summarizing legacy and recent advances in the field. The review emphasizes the interrelated fields of synthesis, characterization, and prediction. Size range 1–100 consists mostly of Bayesian optimization (BO) articles, whereas 101–10 000 consists mostly of support vector machine (SVM) articles. The articles often use combinations of ML, feature selection (FS), adaptive design (AD), high-throughput (HiTp) techniques, and domain knowledge to enhance predictive performance and/or model interpretability. Grouping cross-validation (G-CV) techniques curb overly optimistic extrapolative predictive performance. Smaller datasets relying on AD are typically able to identify new materials with desired properties but do so in a constrained design space. In larger datasets, the low-hanging fruit of materials optimization are typically already discovered, and the models are generally less successful at extrapolating to new mate-

*Corresponding author.
Email address: sparks@eng.utah.edu (Taylor D. Sparks)

rials, especially when the model training data favors a particular type of material. The large increase of ML materials science articles that perform experimental or computational validation on the predicted results demonstrates the interpenetration of materials informatics with the materials science discipline and an accelerating materials discovery for real-world applications.
Keywords: machine learning, validation, extrapolation, dataset size, materials science, chemistry, experimental validation, computational validation, domain knowledge, Bayesian, support-vector machine, adaptive design, high-throughput, grouping cross-validation, feature selection

1. Introduction to Experimental and Computational Machine Learning Validation

Data-driven materials science is plagued by sparse, noisy, multi-scale, heterogeneous, small datasets in contrast to many traditional machine learning (ML) fields [51]. The budding field brings together experts from both materials science and ML disciplines; a great challenge is to incorporate domain knowledge with the appropriate ML tools to discover new materials with better properties [52]. When predictions of new materials are made, experimental or computational validation of those results is less common in the sea of ML articles. This perhaps stems from a requirement to mesh deep expertise from two topics (e.g. density functional theory (DFT) and artificial neural networks (ANNs)) and the difficulty in publishing if validation results do not align with the proposed model or do not produce exemplary results [21].

Some have addressed the former issue of interdisciplinary expertise requirements by providing user-friendly web apps [5] or clearly documented install and use instructions for code hosted on sites such as GitHub [53]. An example of this was the work by Zhang et al. [36], which used a previously constructed ML web app[5] (`http://thermoelectrics.citrination.com/`) which takes only chemical formulas as inputs and went on to validate these predictions of low thermal conductivity for novel quaternary germanides.

The expertise issue is aided by advances in flexible code packages in e.g. Python (`PyTorch` [54], `scikit-learn` [55], `COMBO` [56], `pymatgen` [57], `Magpie` [58], `JARVIS` [59]), MATLAB (`Statistics and Machine Learning Toolbox` [60], `Deep Learning Toolbox` [61]), and R (`caret` [62], `e1071` [63], `nnet` [64]) (see also Table 2 of Butler et al. [65]), which shifts some of the burden of computational optimization, speed, and flexibility away from materials scientists and engineers. Additionally, experimental

(e.g. arc melting [5, 10, 26, 30, 33, 35, 66] and combinatorial magnetron sputtering (CMS) [11, 22]) and computational (e.g. DFT [39–42, 44–49] and finite element method (FEM) [67, 68]) high throughput techniques and materials databases/tools such as the Materials Project [69], Open Quantum Materials Database [70], Pearson's Crystal Database [71], Matminer [72], Dark Reactions Project [21], 2D Perovskites Database, Energy Materials Datamining, and a battery materials database (see also Table 3 of Butler et al. [65]) are available. These techniques, databases, and tools allow for consistent, curated datasets to be more easily produced, accessed, and added to. Thus, for experimental and computational scientists and engineers, an in-depth knowledge of ML algorithms or experimental/computational data production methods may not be necessary to leverage data-driven materials predictions. However, it is likely that when datasets are used for materials discovery, an understanding of the strengths and weaknesses of various algorithms, effect of parameters, and database entry details will improve prediction results. Some publications may also give recommendations of potential, promising compounds for the materials community which are then open for other groups to test [40].

Meredig [51] brought up five high impact research areas for materials science ML, namely: validation by experiment or physics-based simulation, ML approaches tailored for materials data and applications, high-throughput (HiTp) data acquisition capabilities, ML that makes us better scientists, and integration of physics within ML and ML with physics-informed simulations. Oliynyk and Buriak [73] describe 26 articles validated by either experiment or DFT simulation, and Saal et al. [74] give a summary of information from 23 validation articles (all of which are included in the 26 references of [73]) and discuss the five topics in [51]. They point out case studies of appropriately matching an algorithm to a training set for a given prediction type and mention the influence of dataset size on choice of algorithm.

In this work, we sort experimentally and computationally validated articles into three categories based on training dataset size — 1–100 (Section 2.1), 101–10 000 (Section 2.2), 10 000+ (Section 2.3) — and discuss trends and unique examples within each. We then discuss cross-validation (CV) approaches geared towards materials discovery (Section 3) and the pursuit of extraordinary materials predictions (Section 4).

We will assume that the reader is familiar with the basic ML algorithms discussed in this work. For a treatment of these algorithms, we refer the reader to Butler et al. [65].

2. Training Dataset Size Organization of Validation Articles

To our knowledge, no work before has organized and analyzed the corpus of materials informatics literature as a function of dataset size. However, this could be an appropriate way to organize the literature. After all, different algorithms are certainly better suited for different training data sizes. For example, ANNs are commonly referred to as data hungry, whereas others such as Gaussian process regression (GPR) are well-suited to small datasets and generally require sparse approximations for large datasets. We take a rigorous approach by summarizing and comparing 50 validation articles for three training dataset size ranges, 1-100 (Section 2.1), 101-10000 (Section 2.2), and 10 000+ (Section 2.3), identifying the most common methods used for each, highlighting unique approaches, and commenting on general trends with respect to data.

Some articles [24, 29, 32] showed ambiguity with respect to interpreting training dataset size, which could potentially place the article into multiple size ranges for which we take a case-by-case approach. We assign [29, 32] to the 1–100 size range and [24] to the 10 000+ size range.

2.1. 1–100 *Training Datapoints*

ML articles that use less than 100 training datapoints [4, 9–11, 14, 23, 25, 27–29, 31–33, 40–42, 49, 50, 75] are typically Bayesian optimization (BO) and BO/adaptive design (AD) techniques [9–11, 14, 27, 28, 31, 32, 50], with some support vector machine (SVM) [4, 33, 40, 42] among others (e.g. symbolic regression (SR) [29] and random forest (RF) [27]). This is to be expected, as BO and AD techniques can allow fewer experiments to be performed while maximizing the exploratory (probing high uncertainty regions) and exploitative (probing favorable prediction regions) gains of optimization. BO techniques benefit from the inherent availability of uncertainty quantification in addition to property predictions. This can be used for uncertainty quantification through models and offer better explanation of results that deviate from predictions or confirmation of results in areas with low uncertainty and high predictive accuracy. Uncertainty can also be quantified with varying degrees of success for other methods (e.g. bootstrapping SVM results [1, 27, 30, 33]). We now share examples of experimental [4, 9–11, 14, 23, 25, 27–29, 31–33] and computational [40–42, 49, 50] validation articles, first addressing BO and AD (Section 2.1.1) followed by those of other ML types (Section 2.1.2).

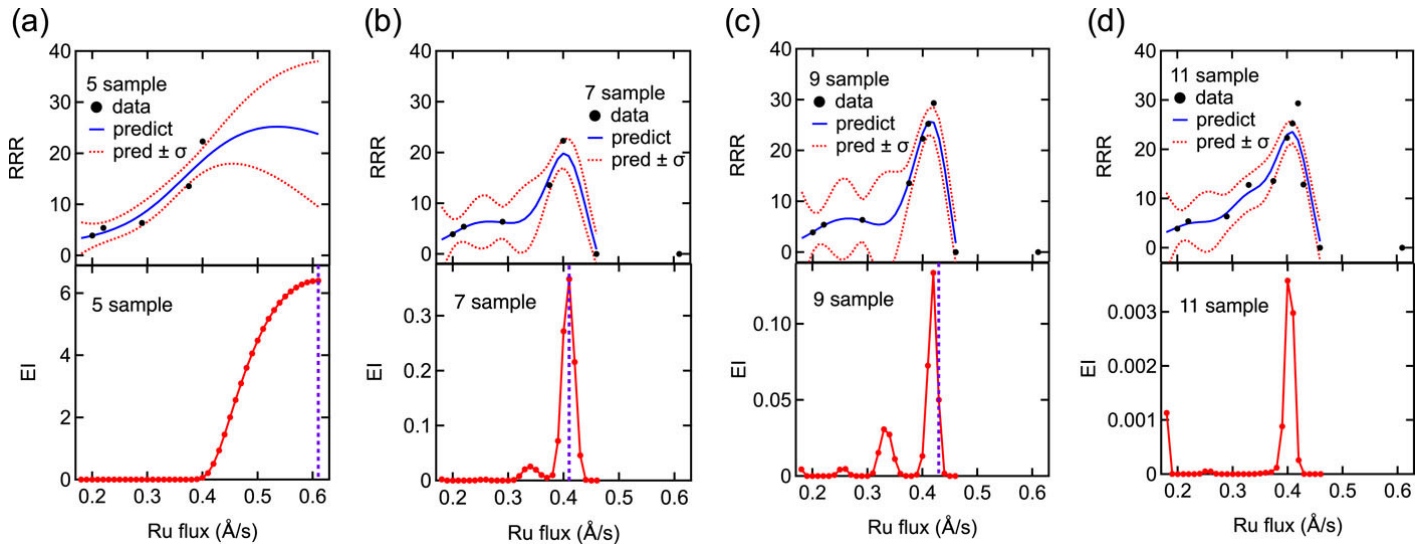

Figure 1: Sequential (i.e. one-variable-at-a-time) Bayesian optimization (BO)/adaptive design (AD) results. Experimental and predicted residual resistivity ratio (RRR), defined as the ratio of resistivity at 300 K to that at 4 K, for 5 random (a), 7 (b), 9 (c), and 11 (d) samples (#6-11 via AD) and expected improvement (EI) values for which the maximum gives the next experiment to perform in the BO/AD algorithm. Uncertainty tends to decrease in regions near new AD datapoints. Reproduced from Wakabayashi, Y. K.; Otsuka, T.; Krockenberger, Y.; Sawada, H.; Taniyasu, Y.; Yamamoto, H. APL Materials 2019, 7 (10)[28]; licensed under a Creative Commons Attribution (CC BY) license (http://creativecommons.org/licenses/by/4.0/).

2.1.1. Bayesian Optimization (BO) and Adaptive Design (AD) Techniques

Wakabayashi et al. [28] seeks to improve the residual resistivity ratio (RRR) (ratio of resistivity at 300 K to that at 4 K), which is a good measure of the purity of a metallic system, of molecular beam epitaxy (MBE) deposited single-crystalline $SrRuO_3$ thin films. Eleven sequential runs per parameter for three parameters in a GPR/AD scheme over 33 total growth runs were used. Maximization of expected improvement (EI) gave the next experiment (Figure 1), as is common to many GPR implementations. First, 11 runs were used to optimize the Ru flux rate, followed by 11 runs to optimize the growth temperature, and finally 11 runs to optimize the O_3-nozzle-to-substrate distance. The highest RRR of 51.79 was obtained relative to the highest value ever reported of 80. Wakabayashi et al. [28] comment that a GPR/AD optimization in 3-dimensional space can be used to further increase the RRR. Naturally, the global optimum is constrained by the scope of the design space, as defined by the three parameters used, their upper and lower bounds, and the resolution used, with trade-offs in the complexity and costs associated with additional experiments.

Wahab et al. [27] performed 4-dimensional simultaneous optimization to increase the Raman G/D ratios (ratio of the height of the D peak, $1350\,\mathrm{cm}^{-1}$, relative to the height of the G peak, $1580\,\mathrm{cm}^{-1}$)

of laser-induced graphene films. Higher G/D ratios indicate better crystallinity and therefore less laser ablation damage. Within 50 optimization iterations, a fourfold increase of Raman G/D ratios (indicating degree of graphitization) relative to common literature values was attained. Twenty initial training datapoints were used, totalling 70 experiments. Instrument precision, gas availability, and user-defined lower and upper limits defined the design space per Table 1, which again, constrain the global optimum. While three of the four optimization parameters are technically non-negative continuous variables (i.e. all except gas type), this is a case where instrument resolution constraints dictate a finite number of testable combinations, which we calculate by the Cartesian product to be $554 \times 195\,000 \times 100 \times 3 = 32\,409\,000\,000$. While the total possible number of combinations is large, this finite number only takes on meaning in the context of a minimum correlation length within the true property-design space; if subtle variations in the parameters cause large changes in Raman D/G ratios, this is indicative of a small correlation length and that many more parameter combinations would need to be tested in a brute force approach.

The more likely scenario is that a slight change in e.g. irradiation power is unlikely to produce a significant change in Raman G/D ratios, as the relatively smooth trends exhibited in the partial dependence plots of Figure 6 of [27] suggest. Kernel scale or correlation length (also referred to as smoothness length) is often a hyperparameter of BO methods, for which a proper choice can greatly affect the rate at which a sequential optimization improves property predictions and approximates the true property-design space. This is an important case where domain knowledge can play an important role, such as by imposing initial conditions or constraints on the kernel scale or other hyperparameters such as property standard deviation. Even in non-BO algorithms, estimations of the local smoothness of the true function being predicted gives context to large combinatoric metrics given in some property-design ML articles; a large number of possible parameter combinations (especially of arbitrarily discretized variables that would otherwise be continuous) does not necessarily correlate with high model complexity if the design space has large correlation lengths.

Homma et al. [9] give another effective and straightforward application of BO in pursuit of enhanced Li-ion conductivities in hetereogenous ternary Li_3PO_4–Li_3BO_3–Li_2SO_4 solid electrolytes. The ternary mixture is adaptively tuned, beginning with 15 gridded training data, followed by 10 AD iterations and yielding a compound 3x higher than any binary composition. Such BO/AD approaches are becoming

Table 1: Parameter space limits for Bayesian Model-based Optimization (MBO) of laser-induced graphene Raman G/D ratio maximization. Reproduced with permission from Wahab, H.; Jain, V.; Tyrrell, A. S.; Seas, M. A.; Kotthoff, L.; Johnson, P. A. Carbon 2020, 167, 609–619. [27].

Parameters	Lower Limit	Upper Limit	Instrument Precision	Number possible values
CW-laser power (W)	0.01	5.55	0.01	554
Irradiation time (s)	0.500	20.000	0.001	195 000
Gas pressure (kPa)	0	6894.76	68.9476	100
Gas type	Argon Nitrogen Air		-	3

increasingly accessible by experimentalists due to the increasing number of powerful, easy-to-use code packages such as COMmon Bayesian Optimization (COMBO) [56] as used in [9] and the similarity with design of experiments (DoE), a familiar technique to many experimentalists.

Li et al. [14] used GPR to predict the optimal doping ratio of Mn^{2+} ions in CZTSSe solar cells, experimentally achieving a highest solar cell efficiency of 8.9%. Four training datapoints and two AD iterations were used where all training data were a multiple of 5%. It appears that the solar cell exhibits a single peak as a function of dopant ratio, suggesting a smooth and simple underlying function which is predicted.

Hou et al. [10] used the GPR implementation in COMBO to maximize the power factor of $Al_{23.5+x}Fe_{36.5}Si_{40-x}$ thermoelectrics by 40% at 510 K relative to their starting sample ($x = 0$) via tuning the Al-Si ratio (x). Forty-eight training datapoints were used across two variables, namely temperature (measured at approximately fixed spacing between 300 K and 850 K) and Al/Si ratio (x).

Wu et al. [31] employed Bayesian molecular design paired with transfer learning towards discovering high thermal conductivity polymers. The Bayesian molecular design strategy generated a library of potential polymer structures by representing polymer structures digitally via a simplified molecular-input line-entry system (SMILES) string. For example, phenol (C_6H_6O) would be represented as `C1=CC=C(C=C1)O`, encoding double bonds as `=`, start and terminal of ring closures by common digits such as `1`, and side chains via parentheses enclosures. They imposed prior information that reduced sampling probability of chemically unfavorable or unrealistic structures and sampled the updated distribution by a sequential Monte Carlo (SMC) scheme. Twenty-eight training structures with thermal conductivity data were used (total 322 observations), and 5917 and 3234 structures were used for the surrogate properties of glass transition temperature and melting temperature, respectively. The trans-

fer learning approach improves mean absolute error (MAE) from $0.0327\,\mathrm{W\,mK^{-1}}$ to $0.0204\,\mathrm{W\,mK^{-1}}$ as shown in parity plots (Figure 2c, Figure 2d), and surrogate model parity plots are also shown (Figure 2a, Figure 2b). Additionally, they synthesized three predicted polymers and demonstrated experimental thermal conductivities similar to state-of-the-art polymers in non-composite thermoplastics.

Talapatra et al. [50] used an extension of the typical GPR scheme in a Bayesian model averaging (BMA) approach. Rather than select a single model for a small training dataset, a weighted average of GPR models with different parameters was used. The weights were assigned based on the prior probability and likelihood of the observed data for each model, and the weights were updated as more data was iteratively added (i.e. the likelihood of the observed data for each model was updated). As the number of observations increases, it is expected that better predictive models progressively are weighted more heavily and that the BMA model predictions improve. Because their BMA implementation depends on many individual GPR models, without sparse approximations, such an approach may be limited to small datasets for which many GPR models can be fitted efficiently. The BMA approach was applied to polycrystalline nanolaminates ternary layered carbides/nitrides. These are also called $M_{n+1}AX_n$ (MAX) phases, where M is a transition metal, A is an A group element, X is C and/or N, and n = 1–3 [76]. They performed single-objective optimization of maximal polycrystalline bulk modulus and minimal shear modulus structures (DFT-based values) and multi-objective of maximum bulk and minimum shear modulus. Six feature sets were used as the candidate models for averaging based on domain knowledge. The authors used 10 initial training DFT simulations and a budget of 70 DFT optimization iterations where a second-order BMA approximation is used. Both maximizing bulk modulus and minimizing shear modulus revealed that the best model almost always had the highest weight, indicating to us that hyperparameter optimization (e.g. choice of feature set) via an appropriate acquisition function (e.g. EI) may be sufficient and yield faster convergence than BMA. However, it remains to be seen if BMA effectively safeguards against poor models better than a (simpler) single hyperparameter optimization step near the beginning of an AD process; poor models rarely have high weight coefficients for the considered dataset, especially when at least 10 training datapoints are available.

Xue et al. [32] incorporated domain knowledge in the form of a quadratic equation describing a phase boundary of interest based on Landau-Devonshire theory into a BO scheme in pursuit of more vertical

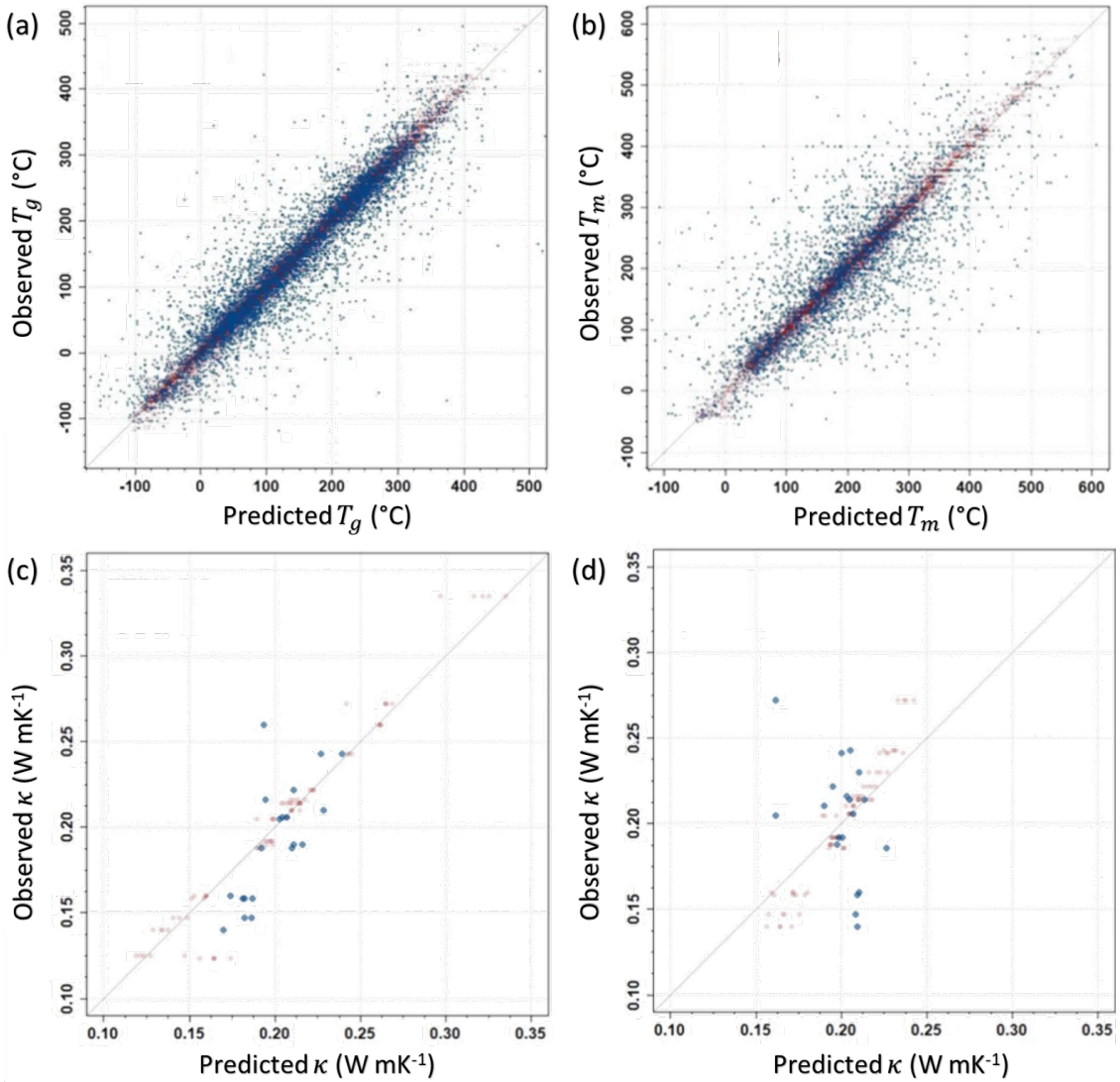

Figure 2: Transfer learning results for a Bayesian molecular design of polymer structures. Glass transition temperature and melting temperature act as proxy models for thermal conductivity and for which parity plots are shown in (a) and (b), respectively. Use of transfer learning enhances prediction accuracy relative to a direct learning approach for which parity plots are shown in (c) and (d), respectively. Adapted from Wu, S.; Kondo, Y.; Kakimoto, M.; Yang, B.; Yamada, H.; Kuwajima, I.; Lambard, G.; Hongo, K.; Xu, Y.; Shiomi, J.; Schick, C.; Morikawa, J.; Yoshida, R. npj Comput Mater 2019, 5 (1), 66[31]; licensed under a Creative Commons Attribution (CC BY) license (http://creativecommons.org/licenses/by/4.0/).

morphotropic phase boundarys (MPBs) in Pb-free $BaTiO_3$-based piezoelectrics. State-of-the-art Pb-free $BaTiO_3$-based piezoelectrics exhibit large electromechanical responses; however, they also exhibit high temperature sensitivity. More vertical MPBs are correlated with less temperature sensitivity, providing motivation for the work in Xue et al. [32]. They used 19 training phase diagrams based on 231 experiments, 83 of which were used as inputs and served the sole purpose of obtaining a fit to the quadratic equation for each phase diagram. Six features based on atomic, crystal chemistry, and electronic structure properties were considered. They successfully predicted and synthesized a piezoelectric with 15 % less curvature in the MPB and lower temperature sensitivity. An important measure of electromechanical response is the longitudinal piezoelectric strain coefficient (d_{33}) for which higher values are more favorable. While d_{33} values around 500–600 $\mathrm{pC\,N^{-1}}$ have been achieved and are present in the initial training data (the performance being a partial motivator for Pb-free $BaTiO_3$-based piezoelectrics), the synthesized material exhibits a d_{33} value of 85 $\mathrm{pC\,N^{-1}}$, highlighting an opportunity to use multi-objective optimization to create a material with both large d_{33} and low temperature sensitivity.

Iwasaki et al. [11] employ a state-of-the-art, accurate, interpretable ML method called factorized asymptotic Bayesian inference hierarchical mixture of experts (FAB-HMEs), which "constructs a piecewise sparse linear model that assigns sparse linear experts to individual partitions in feature space and expresses whole models as patches of local experts" [11]. They use 21 training datapoints and 17 predictors to identify and synthesize a spin-driven thermoelectric (STE) material with the largest spin-driven thermopower measured to date and provide possible insights into new domain knowledge. Thermopower, or the Seebeck coefficient, gives a measure of the voltage induced by a thermal gradient and higher thermopower leads to better performance of thermoelectric generators and coolers. While the first 14 features come from DFT calculations, it is important to realize that the DFT parameters were set up based on experimental composition information from X-ray fluorescence (XRF) and experimental crystal structure information from X-ray diffraction (XRD). They took XRF and XRD data at different points along a "[compositional] spread thin film" made via a CMS technique (HiTp). "For instance, fcc, bcc, and L1_0 structures are the possible crystal structures in FePt binary alloy, which were determined by the combinatorial XRD experiments" (from Supporting Information of [11]). Features 15-17 are experimental; they cut the sample into small sections and measured thermopower. Their approach is

reminiscent of a digital twin, where an object goes through complementary simulation and experimental testing. Their validation was experimental, yielding a material with a thermopower of approximately $13\,\mu\mathrm{V\,K^{-1}}$ compared to to typical state of the art STEs thermopowers below $10\,\mu\mathrm{V\,K^{-1}}$. The authors argue that the interpretable and visualizable FAB-HMEs model they generated (Figure 3) allowed them to discover new insight that thermopower (S_{STE}) and the product term (X_2X_8) of Pt content (X_2) and Pt spin polarization (X_8) are positively correlated. They suggest that ML could be useful in observing previously unexplained phenomena.

2.1.2. Non- Bayesian Optimization (BO)

Other ML methods used in the 1-100 training dataset size include SR [29], SVM [4, 33, 40, 42], polynomial regression (PR) [33], and RF [27].

In a SR scheme, Weng et al. [29] randomly generated 43 000 000 symbolic equations and used these to predict and synthesize 13 new perovskites based on lowest ratio of octahedral factor (μ) to tolerance factor (t), a new descriptor (μ/t) they identified by visually analyzing equations on the Pareto front of MAE vs. equation complexity. Five of the thirteen synthesized perovskites turned out to be pure, and four out of those five are among the highest oxygen evolution reaction (OER) perovskites, where high OER correlates with better catalytic performance of perovskites in e.g. water-splitting into hydrogen or metal-air batteries. Training data consisted of 90 datapoints across 18 in-house synthesized, well-studied, oxide perovskite catalysts (18 perovskites $\times$ 4 samples $\times$ 3 measurements $\times$ 5 current densities = 1080 measurements). Because MAE was used as the metric in the approach, from a model perspective, using a set of repeated measurements of a given perovskite and current density as training data is identical to using the average of the set. Naturally, using repeated measurements across multiple samples to decrease observed noise in the average measured property likely improved the final results of their model and is certainly a wise practice when feasible. Their implementation of SR involved a genetic algorithm approach according to Figure 2b of [29]. With this global optimization approach, a Pareto front of MAE vs. complexity for 8460 mathematical formulas was generated from which they identified and studied the recurring μ/t descriptor and generated a list of promising perovskite compounds based on minimizing μ/t.

Balachandran [40] applied SVM using 18 training datapoints and a single test datapoint from exper-

(a)

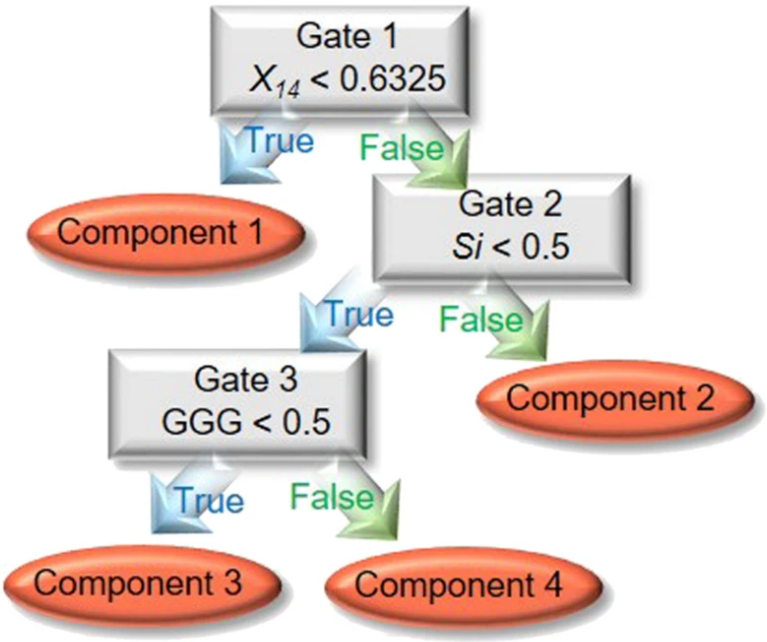

(b)

Component 1 (Non-magnetic materials) $S_{STE} = 0$
Component 2 (Magnetic materials on Si substrate) $S_{STE} = -0.754X_2X_3 + 0.166X_7^2 + 0.173X_1X_8 + 0.348X_2X_8 + 0.491X_1X_{13} - 1.52X_6X_{13} + 0.63X_{11}X_{14} + 0.543$
Component 3 (Magnetic materials on AlN substrate) $S_{STE} = 0.763X_2X_8 + 0.554X_1X_{13} - 2.41X_6X_{13} - 1.52X_{14}X_2 + 0.961X_{11}X_{14} + 2.19$
Component 4 (Magnetic materials on GGG substrate) $S_{STE} = 0.0539X_2X_8 - 0.0111X_6X_{13} - 0.654$

Figure 3: An interpretable model produced by a state-of-the-art ML method, factorized asymptotic Bayesian inference hierarchical mixture of experts (FAB-HMEs), which can be summarized/visualized via a tree structure with components (i.e. regression models) (a) that are accessed by gates (a). Regression models for the four components selected via a Bayesian approach (b). Reproduced from Iwasaki, Y.; Sawada, R.; Stanev, V.; Ishida, M.; Kirihara, A.; Omori, Y.; Someya, H.; Takeuchi, I.; Saitoh, E.; Yorozu, S. npj Computational Materials 2019, 5 (1), 6–11.[11]; licensed under a Creative Commons Attribution (CC BY) license (http://creativecommons.org/licenses/by/4.0/).

imental literature to enhance helical transition temperature of known B20 compounds for spintronics applications via elemental substitution. DFT validated the prediction that Sn can enhance the transition temperature of Fe(Ge,Sn) compounds and they suggest certain experiments for other researchers to perform. Balachandran et al. [42] employed SVM to predict breaks in spatial inversion symmetry due to displacement of cations using 14 published DFT training data and made 10 predictions for materials without existing DFT data which they then validated by DFT. This is useful for identifying promising ferroelectrics because of a correlation between ionic displacement magnitude and Curie temperature, where a high Curie temperature is desired for applications such as ferroelectric capacitor-based computer RAM and heat sensors.

Chen et al. [4] performs a multi-objective, AD optimization to increase the strength and ductility of an as-cast ZE62 (Mg6 wt.% Zn-2 wt.% RE (Y, Gd, Ce, Nd)) Mg alloy, which is of interest for aerospace, vehicle, electronic, and biomedical applications due to low density, high stiffness, and high biocompatibility. Ten initial training datapoints selected by orthogonal design are used to train a SVM model, followed by iterative recommendations of next parameters for a four-parameter experiment via either a Pareto front vector or scalarization approach. In the Pareto front vector approach, the angle between two vectors w^t and w^p is minimized, where w^t and w^p are vectors from the origin to the target and the virtual (i.e. SVM-based) Pareto front, respectively. The target point used in their work was 15.6 % strain and 157.2 MPa yield strength, as obtained via Figure 2c of [4] and DataThief III [77]. In the scalarization approach, a point in the virtual space with minimum distance to the target is found. In either approach, when minimization is complete, the minimized point in the virtual space defines the set of parameters for the next experiment. Both approaches performed similarly, and the latter gave a material with strength and ductility improved by 27% and 13.5%, respectively, relative to the initial training dataset via 4 iterations of experiments.

While Wahab et al. [27] falls primarily into the category of BO and was discussed in Section 2.1.1, a RF surrogate model with 500 trees is used due to the presence of both continuous numerical and discrete categorical variables; however, it is worth noting that GPR and other methods can handle both types simultaneously via dummy variables [78].

Sendek et al. [49] demonstrated a new large-scale computational screening method capable of iden-

tifying promising candidate materials for solid state electrolytes for lithium-ion batteries. First, 12 831 lithium containing crystalline solids were screened for high structural and chemical stabilities, low electronic conductivity, and low cost down to 300 potential candidates. A training set of 40 crystal structures and experimentally reported ionic conductivity values from literature were used to train a superionic classification model using logistic regression to identify which of those candidate structures are most likely to exhibit fast lithium conduction. They identify a 5-feature model, selected from 20 potential atomic and chemical property features, that resulted in the lowest cross-validated misclassification rate (CVMR) and training misclassification rate (TMR) of 10 % (in other words, 4 of the 40 training points are misclassified). From the 300 potential candidates, the model narrowed that down to 21 crystal structures that showed promise as electrolytes. Sendek et al. [49] concluded that a multi-descriptor model exhibits the highest degree of predictive power, compared to stand alone simple atomistic descriptor functions, and it also served as a first step towards a robust data-driven model to screen for promising solid electrolyte structures.

Xue et al. [33] trained five different iterative statistical learning models to make rapid predictions of the transformation temperature of NiTi-based alloys from a training set of 53 synthesized alloys and three features (Pauling electronegativity, metallic radius, and Waber Cromer's pseudopotential radii). A bootstrap resampling method was applied to the dataset with 53 points and used to train a linear regression (LR), PR, SVM with a radial basis function (RBF) kernel, SVM with a linear kernel, and SVM with a polynomial kernel. Using validation from a high precision testing dataset with 23 points on the transformation temperatures of NiTi-based shape-memory alloys, the PR model had the lowest error out of the 5 with a mean square error (MSE) of about 40 °C. Next, an adaptive design loop used a trade-off between exploration and exploitation to find the highest transformation temperature alloy in the virtual dataset consisting of 1 652 417 unexplored alloys. Three different selectors (max, efficient global optimization (EGO), and Knowledge Gradient (KG)) were employed for two iterations to improve the virtual dataset by suggesting the next candidate material for experiment. Experimental validation found that the PR model significantly improves after the virtual dataset is improved (the MSE decreases from 15.7 °C to 15.0 °C). Xue et al. [33] demonstrated a systematic learning and adaptive design framework that can guide future synthesis and discovery of new materials with certain desired properties.

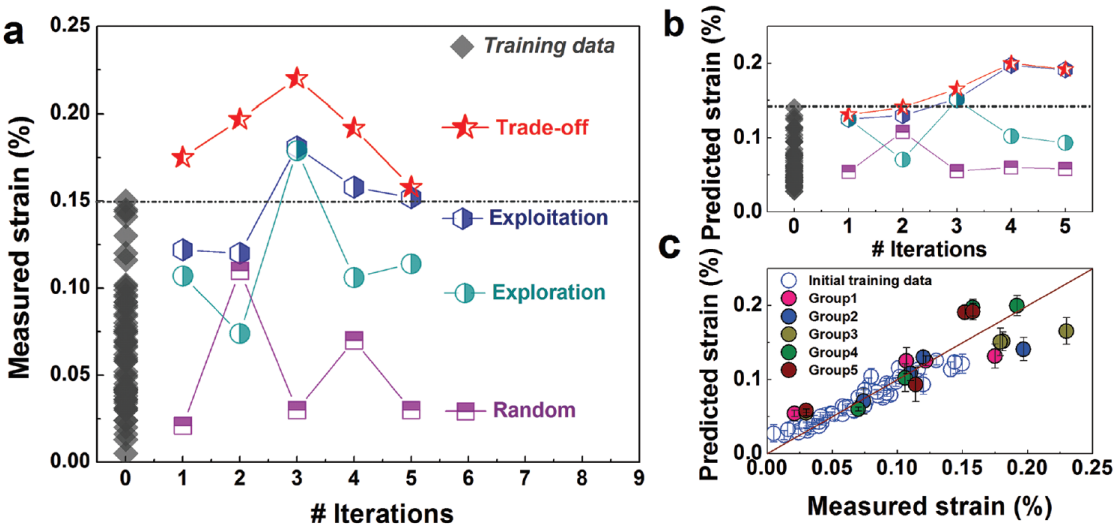

Figure 4: Overall performance of the trade-off between exploration (probing high uncertainty) and exploitation (probing high performance) design methodology. (a) The trade-off between exploration and exploitation methodology gives higher measured electrostrain (%) in comparison with the other four design methodologies for an increasing number of iterations. (b) Predictions made from the model using the trade-off strategy. (c) Parity plot showing the accuracy of the trade-off model's predicted strains % in comparison to new synthesized compounds. Reproduced with permission from Yuan, R.; Liu, Z.; Balachandran, P. V.; Xue, D. D.; Zhou, Y.; Ding, X.; Sun, J.; Xue, D. D.; Lookman, T. Advanced Materials 2018, 30 (7).[34]

Yuan et al. [34] used an SVM model with a RBF kernel and 61 experimental training datapoints to discover new Pb-free $BaTiO_3$ (BTO) based piezoelectrics with large electrostrain. The model screened 605 000 unexplored compositions and performed five AD iterations in sets of four experiments. Validation compounds were experimentally synthesized following predictions from four strategies: exploitation, exploration, trade-off between the former two, and random selection (Figure 4). An optimized trade-off between exploration (high uncertainty regions) and exploitation (best predicted performance regions), was achieved by experimentally comparing multiple design strategies. Thus, they were able to produce an optimal criterion for the synthesis of the piezoelectric $(Ba_{0.84}Ca_{0.16})(Ti_{0.90}Zr_{0.07}Sn_{0.03})O_3$, for which the largest electrostrain was 0.23 % in the BTO family. The trade-off between exploration and exploitation is especially significant because it provides a good precedent in guiding experiments in materials design.

2.2. 101–10 000 *Training Datapoints*

Many of the ML validation articles that have 101-10000 training datapoints [1–3, 7, 8, 12, 16–22, 26, 30, 35, 37–39, 44, 45, 48, 68] use SVM [1, 3, 7, 8, 12, 16, 18, 19, 21, 26, 30, 37–39, 44, 68]. There are also other examples such as ensemble [7], ANN [30], RF [12], decision tree (DT) [21, 30], recursive feature elimination (RFE) [37], least absolute shrinkage and selection operator (LASSO) [2], cluster

resolution feature selection (CR-FS) [7, 8, 19], DoE [3], LR [12, 21, 30], PR [30], partial least squares (PLS) [7], matrix-based recommender [48], synthetic minority oversampling technique (SMOTE) [7], k-nearest neighbor (kNN) [7, 21, 30], and kernel ridge regression (KRR) [44] approaches. Of the "other" ML articles, only [2, 17, 20, 22, 35, 45, 48] are not already included in the SVM group, indicating that SVM is often combined or compared with other methods. Most of the SVM articles described here employ a RBF kernel, imposing smooth, Gaussian behavior on the predicted properties. We now share examples of experimental [1–3, 7, 8, 12, 16, 18–22, 26, 30, 35, 37, 38, 68] and computational [39, 44, 45, 48] validation articles, addressing SVM/AD (Section 2.2.1), SVM/CR-FS (Section 2.2.2), general SVM (Section 2.2.3), and non-SVM (Section 2.2.4).

2.2.1. Support Vector Machine (SVM) and Adaptive Design (AD)

Balachandran et al. [1] used SVM and a two-step classification then regression approach with 167 and 117 initial training datapoints, respectively, to predict new high Curie temperature (T_C) xBi[Me_y'Me_y"]O_3–(1-x)$PbTiO_3$ perovskite compounds through 5 iterations of AD. Of the 10 compounds they experimentally synthesized, 6 were perovskites. With an initial approach using only regression and no classification, a perovskite was predicted and synthesized, but discovered to be non-pure. The classification algorithm includes training data from non-pure perovskites and is aimed at identifying promising regions in the four-parameter design space (x, y, Me_y', and Me_y" in xBi[Me_y'Me_y"]O_3–(1-x)$PbTiO_3$) that are more likely to produce pure perovskite phases. The regression step is then aimed at identifying specific compositions with high T_C for ferroelectric applications. In the AD scheme, only compositions which are classified as perovskites are updated in the regression model, and a EGO scheme [79] is used to identify new compositions for synthesis (Figure 5). Since only a single iteration was used for the regression-only approach before switching to a two-step approach, it is unclear to what extent the classification algorithm affected the regression model and subsequent success of choosing high T_C candidates. However, of the six discovered perovskites, 0.2 Bi($Fe_{0.12}Co_{0.88}$)O_3–0.8 PT had the highest experimental T_C of 898 K, and three were novel Me_y'Me_y" pairs: FeCo, CoAl, and NiSn. For comparison, the highest and median T_C perovskites in the training data are approximately 1100 K and 750 K, respectively.

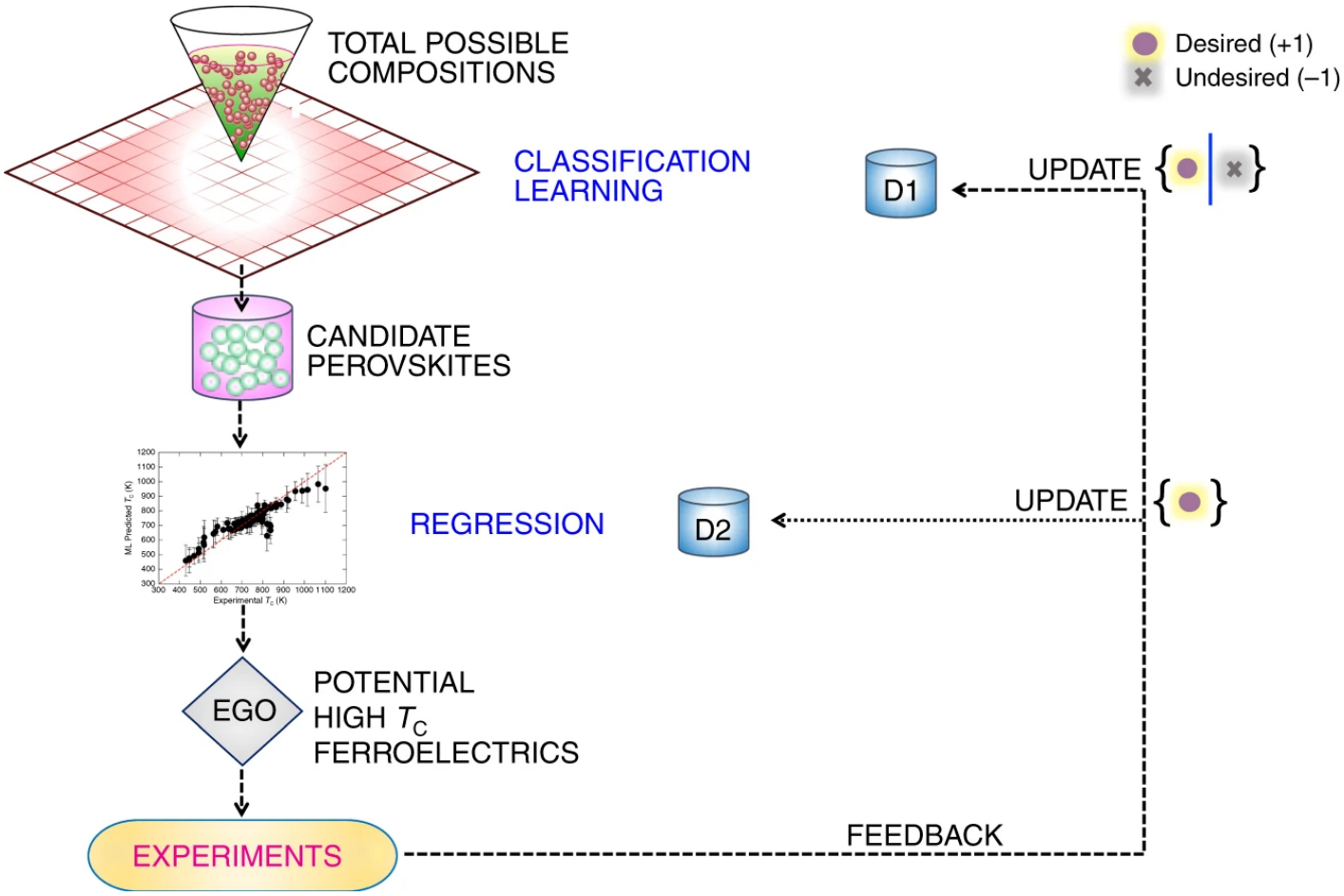

Figure 5: Two-step machine learning algorithm involving adaptive design (AD). Step 1: Screening by classification algorithm to identify perovskite compositions that can be made without impure phases. Step 2: Predict Curie temperature via support vector machine (SVM) regression and identify promising candidates using efficient global optimization (EGO). Both successful and failed experiments train the classification model via AD, for which only successful experiments are passed on to the regression model. Reproduced from Balachandran, P. V.; Kowalski, B.; Sehirlioglu, A.; Lookman, T. Nature Communications 2018, 9 (1)[1]; licensed under a Creative Commons Attribution (CC BY) license.

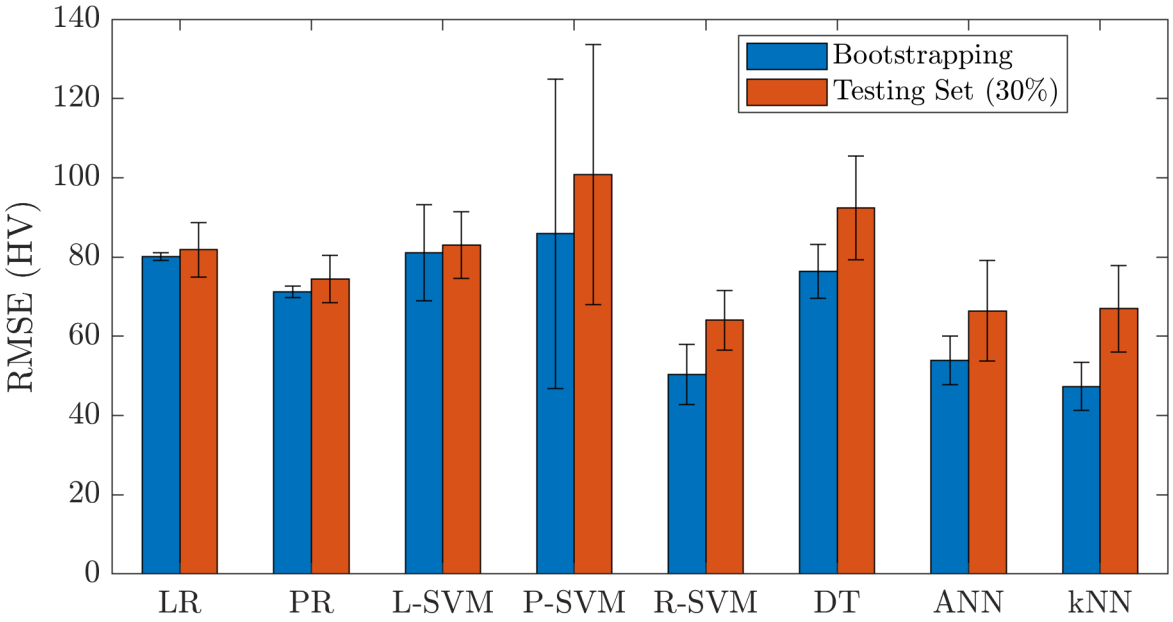

Figure 6: Root mean square error (RMSE) and uncertainty standard deviation for bootstrapped and test set predictions for various models: linear regression (LR), polynomial regression (PR), linear support vector machine (SVM) (L-SVM), polynomial SVM (P-SVM), radial basis function (RBF) SVM (R-SVM), decision tree (DT), artificial neural network (ANN), and k-nearest neighbor (kNN). RBF SVM had the lowest test dataset error and was used as a surrogate model. Reproduced with permission from Wen, C.; Zhang, Y.; Wang, C.; Xue, D.; Bai, Y.; Antonov, S.; Dai, L.; Lookman, T.; Su, Y. Acta Materialia 2019, 170, 109–117.[30] Bar chart data was extracted via https://apps.automeris.io/wpd/ and replotted using MATLAB.

Wen et al. [30] searched for high-entropy alloys (HEAs) having high hardness using 135 training data samples (18 experimentally from their lab) and demonstrated that learning from composition and descriptors exploiting HEA domain knowledge outperformed ML models that use only compositional descriptors. They compared performance across several different models (LR, PR, SVM, DT, ANN, and kNN), for which SVM with a RBF kernel had the best performance on test data (Figure 6). The SVM surrogate model was used in a DoE-based AD scheme and feature selection (FS) was performed via a hybrid correlation analysis (CA)/wrapper. Using arc melting, they synthesized 42 alloys, 35 of them having higher hardness than the hardest candidates of the training set, 17 of them having $\sim$10 % higher hardness, and the highest with $\sim$14 % higher hardness (883 ± 47 HV relative to 775 HV). They suggested extending this framework to bulk metallic glasses and superalloys.

Cao et al. [3] optimized power conversion efficiency of PDCTBT:$PC_{71}BM$ organic photovoltaics via SVM, DoE, and 16 AD iterations using a total of 150 experimental devices to achieve a maximum power conversion efficiency of approximately 7.7 %.

Balachandran et al. [39] used a dataset of 223 M_2AX family of compounds containing information about bulk, shear, and Young's modulus that were calculated using DFT and used it on an iterative ML design strategy composed of two main steps: 1) ML trained a regressor that predicts elastic properties by elementary orbital radii of the individual components of the materials, and 2) a selector used these predictions and their uncertainties to choose the next material to investigate. Additionally, DFT calculations were used to measure the desirability of the properties of a potential materials candidate. Three different regressors, GPR, SVM with a RBF kernel, and SVM with a linear kernel, were compared along with two different selectors, EGO and KG. Ideally, the resulting model should provide a balance between exploration and exploitation and obtain a material with the desired elastic properties in as few iterations as possible. The performance of each model was measured in terms of "opportunity cost" and the number of iterations used to find a material. They found that selectors that use information about the prediction uncertainty perform better than by themselves.

2.2.2. Support Vector Machine (SVM) and Cluster Resolution Feature Selection (CR-FS)

Gzyl et al. [7] predicted half-Heusler structures, compounds with equiatomic proportions *ABC* (important for thermoelectrics, spintronics, and topological insulators), with a sensitivity, selectivity, and accuracy of 88.3 %, 98.2 %, and 97.6 %, respectively. They used 2818 experimental training data points and an ensemble of PLS, SVM, and kNN ML models. Each of the three ML techniques was combined with a CR-FS and genetic algorithm (GA) (also referred to as evolutionary algorithm (EA)) descriptor selection model, giving in total six models (Figure 7a). Additionally, the ensemble classification scheme was combined with SMOTE to address issues of unbalanced datasets and overfitting (Figure 7b). The ensemble classification schemes used soft-voting where predicted probabilities of being half-Heusler were averaged among the six models, and compounds with averaged probabilities above 50 % were classified as half-Heusler (Figure 7c). Six of seven and 7/7 predicted half-Heusler and non-half-Heusler compounds, respectively, were successfully synthesized and confirmed. Once SMOTE had been applied, use of an ensemble approach increased the validation set sensitivity (rate of true positives) from 83.3 % (best individual model, SVM CR-FS) to 88.3 % while maintaining near identical validation specificity and accuracy.

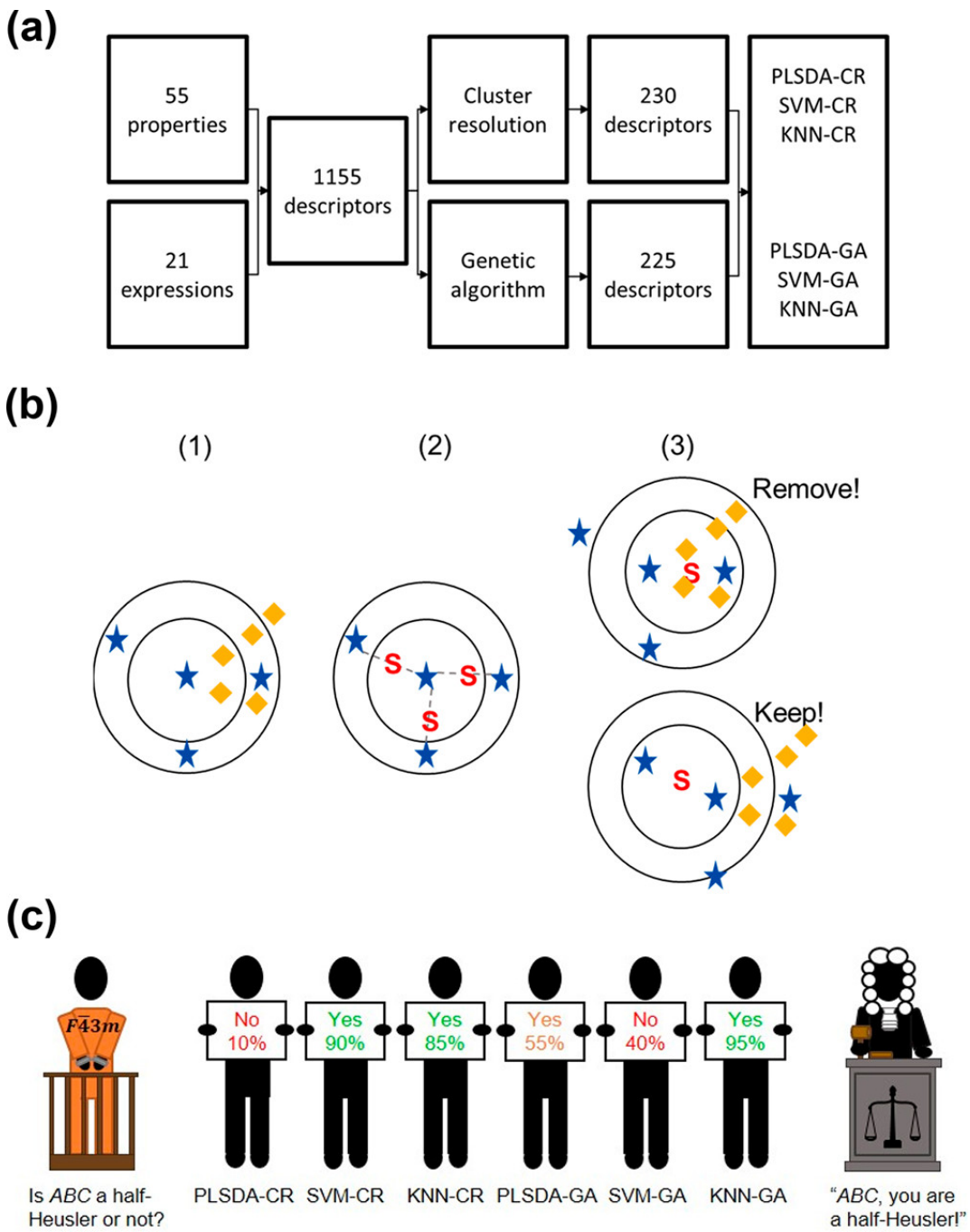

Figure 7: cluster resolution feature selection (CR-FS) and genetic algorithm (GA) approaches selected 230 and 225 descriptors from a set of 1155 descriptors, respectively, and each approach was paired with partial least squares (PLS), support vector machine (SVM), and k-nearest neighbor (kNN), resulting in 6 models (a). synthetic minority oversampling technique (SMOTE) is used to address the issue of imbalanced data, where synthetic samples (S) are generated between pairs of minority (i.e. less frequently occurring) samples (★). If most nearest neighbors to S are minority samples, S is kept, otherwise if most nearest neighbors to S are majority samples (◆), S is removed. Finally, a soft-voting ensemble of the 6 models is used to classify whether a material is half-Heusler or not (yes if >50 %, no if <50 %). Reproduced with permission from Gzyl, A. S.; Oliynyk, A. O.; Mar, A. Crystal Growth & Design 2020.[7]

Gzyl et al. [8] used 179 experimentally reported structures, 23 descriptors (selected via CR-FS from 243 descriptors based on 43 elemental properties), and SVM to classify half-Heusler site preferences resulting in a sensitivity, selectivity, and accuracy of 93%, 96%, and 95%, respectively. One goal of the work was to apply data sanitation by retesting classified candidates with various classification probabilities. Three compounds, MnIrGa, MnPtSn, and MnPdSb, gave probabilities of 0.127, 0.043, and 0.069, respectively, before CR-FS and 0.881, 0.881, and 0.680, respectively, after CR-FS, of which the higher probabilities were more accurate. Thus, using a CR-FS scheme had notable benefits as further demonstrated by better delineation between Heusler and non-Heusler in Figure 8. Two compounds, GdPtSb and HoPdBi, which were considered misclassified based on existing input data, were resynthesized. The results were confirmed for both compounds by powder XRD; additionally, a single-crystal HoPdBi sample was available, for which a full structural determination and unambiguous proof was obtained. This characterization demonstrated that the model's classification was indeed correct while the original input data was not. Revised crystallographic information files (CIFs) were then prepared and submitted to the appropriate database, highlighting a successful example of data sanitation validated by experiment as well as a caution about possible discrepancies in input data.

Oliynyk et al. [19] filtered 990 features down to 113 by CR-FS and applied SVM to 1037 training datapoints of 1:1:1 ternary structures (TiNiSi-, ZrNiAl-, PbFCl-, LiGaGe-, YPtAs-, UGeTe-, and LaPtSi-type). They validated on 19 experimental samples and found that in a "structurally confused" region ($0.3 <= \text{probability} <= 0.7$), both phases can coexist. This indicates that the "confused" region of a properly trained, appropriate classification scheme can indicate more than just sparsity or noisiness of data; it can also point to physical phenomena where either classification type may exist or even coexist.

Oliynyk et al. [18] trained a partial least-squares discriminant analysis (PLS-DA) and SVM to develop a crystal structure predictor for binary AB compounds from 706 AB compounds with the seven most common structure types (CsCl, NaCl, ZnS, CuAu, TlI, $\beta-$FeB, and NiAs) and 31 elemental property features. In predicting crystal structure, PLS-DA and SVM showed an accuracy of 77.1 % and 93.2 %, respectively, after validation. Both models made quantitative predictions of hypothetical compounds. For example, PLS-DA and SVM predicted RhCd to have a CsCl-type structure with 0.669 and 0.918

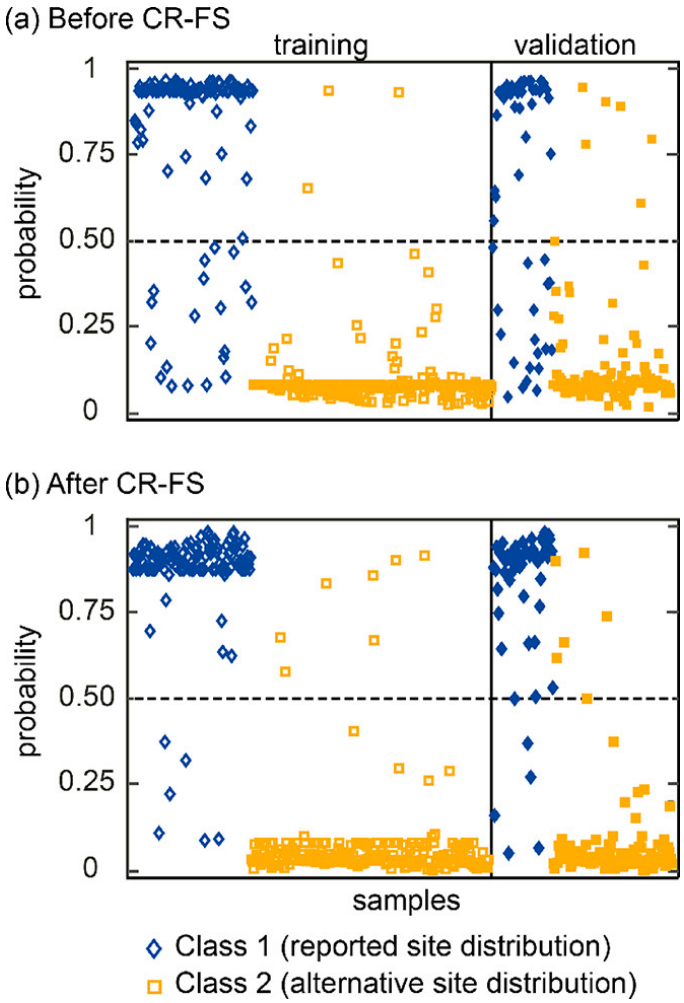

Figure 8: Applying cluster resolution feature selection (CR-FS) improves support vector machine (SVM) classification of reported (class 1) vs. alternative (class 2) site distributions for preferential site distributions in half-Heusler compounds (before CR-FS (a), after CR-FS (b)). A perfect classification accuracy would show all blue diamonds with a probability of 1 and all orange squares with a probability of 0. The algorithm was trained on 119 class 1 datapoints and 239 class 2 datapoints and validated on 60 class 1 datapoints and 119 class 2 datapoints. Reproduced with permission from Gzyl, A. S.; Oliynyk, A. O.; Adutwum, L. A.; Mar, A. Inorg. Chem. 2019, 58 (14), 9280–9289.[8]

probability, respectively, which was then later confirmed after experimental synthesis. Oliynyk et al. [18] concluded SVM is the superior classification method in crystallography that can make quick and accurate predictions on crystal structure and has potential to be applied to identify the structure of any unknown compounds.

2.2.3. General Support Vector Machine (SVM)

Kauwe et al. [12] used 263 chemical formulae (e.g. Al_2O_3) and temperatures from 298.15–3900 K obtained from NIST:JANAF tables (in total 3986 training datapoints) to predict heat capacity (C_p) of inorganic solids with SVM, LR, and RF. Grouping cross-validation (G-CV) was used to test extrapolative prediction (Figure 11), giving C_p root mean square errors (RMSEs) of 21.07 ± 3.60, 19.22 ± 2.40 and $15.15 \pm 2.50\,\mathrm{J\,mol^{-1}\,K^{-1}}$ for SVM, LR, and RF, respectively. This showed significant improvement over conventional Neumann-Kopp (based on summing heat capacities of constituent elements in a chemical formula) and comparable performance to cation/anion contribution (CAC) (based on cation/anion pairs and a temperature dependent power series), the latter of which had 161/263 chemical formulae with available data. Kauwe et al. [12] also noted that CAC likely used many of the same chemical formulae to obtain CAC fitting parameters which probably caused an overestimation of CAC performance. While the RMSE of CAC was on par with the ML methods, the systematic errors and steep over- or under-estimation in some regions (in some cases even with a negative parity slope) highlights the need to consider more than a single metric in evaluating model performance and account for systemic error in the data. Indeed, RF performed much better than CAC across the full temperature range (Figure 9).

Tehrani et al. [26] predicted two ultraincompressible, superhard materials, $ReWC_2$ and $Mo_{0.9}W_{1.1}BC$. The former was synthesized as $ReWC_{0.8}$ due to unreacted graphite in $ReWC_2$ and is a brand-new ultraincompressible, high-hardness material. $Mo_{0.9}W_{1.1}BC$ had been previously studied in the literature and was further confirmed as an inexpensive, earth-abundant, ultraincompressible hard material. They used SVM of 2572 elastic moduli training datapoints from the Materials Project database [69] and 150 descriptors built from arithmetic operations on compositional and structural properties. Training data was curated from an original set of 3248 elastic moduli entries by eliminating inaccessible phases at ambient pressure and temperature and removing unreasonable entries with e.g. negative values, among other restrictions. While the full descriptor set was used for prediction, for perspective, descriptors were

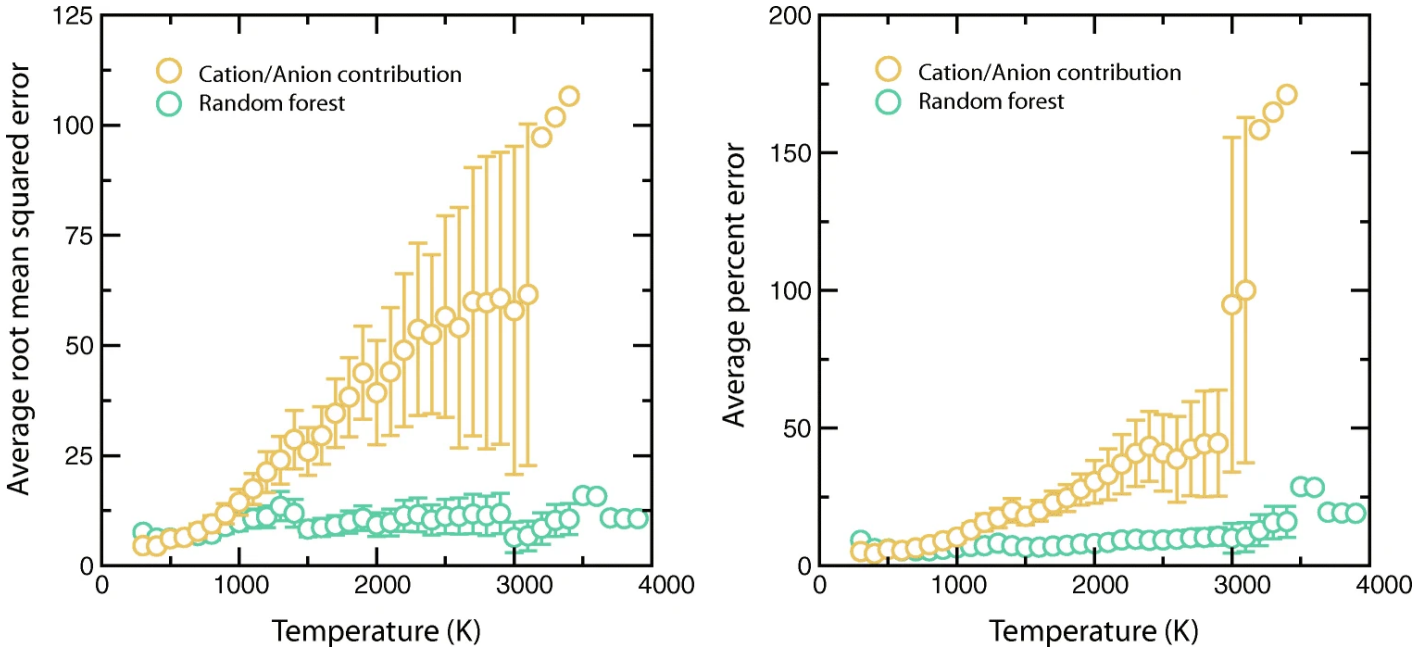

Figure 9: Average RMSE for heat capacity SVM predictions of inorganic solids ($\mathrm{J\,mol^{-1}\,K^{-1}}$) vs. temperature (K), where average RMSE was calculated by averaging temperatures in 100 K increments or groups. 95 % confidence intervals were calculated using cross-validation (CV) metrics. Reproduced from Kauwe, S. K.; Graser, J.; Vazquez, A.; Sparks, T. D. Integrating Materials and Manufacturing Innovation 2018, 7 (2), 43–51[12]; licensed under a Creative Commons Attribution (CC BY) license (http://creativecommons.org/licenses/by/4.0/).

fed through a GA-based FS algorithm, indicating that 52 and 44 % of the descriptors were essential for Bulk modulus (B) and shear modulus (G), respectively. Both B and G correlate positively with hardness and are used as proxies in the approach. Careful attention is paid to trends of errors relative to the compound type being predicted; for example, metallic/covalent bonding materials general exhibit lower error than highly ionic compounds. The SVM model predicts B and G for 120 000 binary, ternary, and quaternary inorganic solids in Pearson's Crystal Database[71] with cross-validated root mean square errors (RMSECVs) of 17.2 and 16.5 GPa, respectively. $ReWC_2$ and $Mo_{0.9}W_{1.1}BC$ are identified as potential high hardness candidates, having the highest predicted B and G out of all ternary ($ReWC_2$) and quaternary ($Mo_{0.9}W_{1.1}BC$) candidates, and were amenable to synthesis via ambient pressure arc melting. Due to presence of unreacted graphite peaks in powder XRD experiments of $ReWC_2$, eventually $ReWC_{0.8}$ was settled on for testing. High-pressure diamond anvil cell (DAC) experiments confirmed ultraincompressibility and Vicker's microhardness experiments confirmed superhardness at low loads, 40 ± 3 and 42 ± 2 GPa for $ReWC_{0.8}$ and $Mo_{0.9}W_{1.1}BC$, respectively.

Raccuglia et al. [21] used in-house "dark" or failed experiments to enhance a SVM model, achieving 89% accuracy relative to 79% accuracy via human intuition. No comparison against a ML model without failed experiments was reported. A web database (https://darkreactions.haverford.edu/) was made publicly accessible for failed chemical reaction experiments.

Zhuo et al. [37] predicted and tested thermal quenching temperature (temperature at which emission intensity is cut in half relative to initial) using SVM and 134 experimental training datapoints. Five compounds (Sr_2ScO_3F, $Cs_2MgSi_5O_{12}$, $Ba_2P_2O_7$, $LiBaB_9O_{15}$, and $Y_3Al_5O_{12}$) had predicted thermal quenching temperatures above 423 K and exhibited thermal stability when using E^{3+} as a substitutional atom.

In earlier work, Zhuo et al. [38] predicted and tested Debye temperature as a proxy for photoluminescent quantum yield (i.e. energy-efficiency of light bulb phosphors) using SVM, 2610 DFT training datapoints, and RFE (FS method) for 2071 potential phosphor hosts. The compound with highest Debye temperature and largest band gap, $NaBaB_9O_{15}$, was synthesised and $NaBaB_9O_{15}$:Eu^{2+} was shown to have a quantum yield of 95 %. The Debye temperature RMSECV and cross-validated mean absolute error (MAECV) was 59.9 and 37.9 K, respectively, with most temperatures of training data between 50–750 K.

Lu et al. [44] combined various ML techniques with DFT calculations to quickly screen hybrid organic-inorganic perovskites (HOIPs) for photovoltaics based on bandgap. Six ML regression methods (gradient boosting regression (GBR), KRR, SVM, GPR, DT regression, and multilayer perceptron regression) were trained using 212 reported HOIPs bandgap values. 14 selected material features were narrowed down from an initial 30 property features (including properties such as ionic radii, tolerance factor, and electronegativity) through feature engineering. The GBR model was shown to be the most accurate, so it was then used to screen 5158 unexplored HOIPs (346 that had been previously studied and 5504 that were calculated) for any promising HOIPs that are both efficient and environmentally sustainable. They successfully screened 6 orthorhombic lead-free HOIPs with proper bandgap for solar cells and room temperature thermal stability, of which two particularly stood out. Validations of these results from DFT calculations showed that the two are in excellent agreement, with the ΔE_g never being larger than 0.1 eV. Lu et al. [44] demonstrated a highly accurate method that can be used on a broader

class of functional materials design.

Min et al. [16] used a dataset of 300 Ni-rich $LiNi_xCo_{1-x-y}Mn_{1-x-y-z}O_2$ cathodes with 13 input variables (synthesis parameters, inductively coupled plasma mass spectrometry, and X-ray diffraction results) to compare the accuracy of 7 different ML algorithms (SVM, DT, ridge regression (RR), RF, extremely randomized tree (ERT) with an adaptive boosting algorithm, and ANN with multi-layer perceptron) in predicting the initial capacity, capacity retention rate (CRR), and amount of residual Li. The ERT with adaptive boosting algorithm resulted in the highest predictive accuracy, with an average coefficient of determinant, R^2, of 0.833. Additionally, Min et al. [16] employed a reverse engineering model to propose optimized experimental parameters that satisfy target specifications. These optimal parameters were then fed into the trained ML model, that makes corresponding electrochemical property predictions based on them. Experimental validations showed average differences of 6.3, 1.0 and 12.8 % for the capacity, CRR, and free Li, respectively.

2.2.4. Non- Support Vector Machine (SVM)

Seko et al. [48] used four descriptor-free recommender systems — non-negative matrix factorization (NMF), singular value decomposition (SVD), canonical polyadic decomposition (CPD), and Tucker decomposition — to predict currently unknown chemically relevant compositions (CRCs). The Tucker decomposition recommender system had the best discovery rate which was validated by performing DFT calculations on phase stability of 27 recommended, unknown candidates, 23 of which were stable (85 % discovery rate).

Ren et al. [22] searched for metallic glasses in the Co−V−Zr ternary system using RF and 315 initial training datapoints, followed by a HiTp CMS, AD scheme producing 1315 total points (including "dark", i.e. failed, experiments). Discrepancies in the initially trained model were used for retraining which improved acccuracy for the Co−V−Zr predictions. Two additional unreported ternaries, Co−Ti−Zr and Co−Fe−Zr, were discovered. A "grouping" CV approach (G-CV) was used for outside-of-dataset predictions (Section 3).

Oliynyk et al. [20] searched for Heusler-type structures using a classification RF model with compositional descriptors and 1948 compounds (341 of which are Heusler) across 208 structure types as training data, achieving a sensitivity (true-positive rate) of 0.94. Of 21 synthesized compounds, 19 were

predicted correctly (12/14 as Heusler and 7/7 as non-Heusler). $TiRu_2Ga$, a potential thermoelectric material, was also synthesized and confirmed to have Heusler structure.

Bucior et al. [2] predicted hydrogen uptake in metal-organic frameworks (MOFs) by predicting 50 000+ compounds via a LASSO approach with 1000 training grand canonical Monte Carlo (GCMC) simulations and 12 binned energy features. The energy features were obtained by overlaying a 3D grid on the GCMC simulation box, probing each grid point with a "hydrogen probe" and binning the 3D distribution into a 1D histogram with 12 bins (1 feature per bin). The predictions were screened by retrieving and running GCMC simulations on the top 1000 predictions. The max GCMC simulation in the training data was $\sim$47.5 g L^{-1} H_2 uptake, and 51 of the top 1000 simulations were >45 g L^{-1}. They synthesized one promising MOF, MFU-4l(Zn), with a predicted $\sim$54 g L^{-1} H_2 uptake (100 bar $\rightarrow$ 5 bar) and experimentally characterized as having 47 g L^{-1} H_2 uptake (100 bar $\rightarrow$ 5 bar) which is competitive with similar experimental MOFs in the literature.

Nikolaev et al. [17] designed an automated method to study the synthesis and target a specified growth rate of single-walled carbon nanotubes (CNTs), called Autonomous Research System (ARES) which is the first to do closed-loop iterative materials experimentation. ARES was capable of designing, executing, and analyzing experiments orders of magnitude faster than current research methods. To achieve this, ARES used a RF/GA planner that was trained off of an initial database of 84 experiments that was then updated as it performed a series of approximately 600 experiments. ARES demonstrated an autonomous research system capable of controlling experimental variables in materials science.

Mannodi-Kanakkithodi et al. [45] trained a KRR-based ML model using the crystal structures of 284 four-block polymers (250 training datapoints and 34 test points), including relevant property information about each: bandgap and ionic and total dielectric constant (calculated from DFT). Additionally, each polymer was fingerprinted based on their building block identities using the Pearson correlation analysis to explore the possibility of a correlation between those fingerprints and a polymer's properties. By validating using DFT calculations and experimental values from synthesized polymers, the KRR model converted a fingerprint to property values with an average error for all three properties mentioned above of 10% or less. A genetic algorithm then searched for materials with desired properties that can then be inputted into the KRR model, instead of traditional approaches like random search and

chemical-rules based search. Mannodi-Kanakkithodi et al. [45] demonstrated how carefully created and curated materials data can be used to train statistical learning models so that they only require a simple fingerprint of a new material to predict its properties. Furthermore, they also showed that the combination of a genetic algorithm with learning models can efficiently determine specific materials that possess certain desired properties.

Zhang et al. [35] extracted 1062 experimentally measured load-dependent Vickers hardness data from literature and 532 unique compositions to train a supervised RF algorithm using boosting algorithms (gradient boosting decision tree (GBDT) and XGBoost). The RF model's hardness predictions were validated using two different hold-out test sets: the first with Vickers hardness measurements for 8 synthesized, unmeasured metal disilicides and the second with a customized hold-out containing several classic high hardness materials. After validation, the model screened more than 66 000 compounds in the crystal structure database, of which 10 are predicted to be superhard at 5 N. Due to the low number of entirely new predicted materials (most had already been discovered), the hardness model was combined with a recently developed formation energy and convex hull prediction tool to find new compounds with high hardness. More than ten thermodynamically favorable compositions with hardness above 40 GPa were discovered, proving that this model can successfully identify completely new materials with extraordinary mechanical properties.

2.3. 10 000+ *Training Datapoints*

Experimentally and computationally validated ML articles that use more than 10 000 training datapoints are sparse compared to the previous two training datapoint set sizes considered in this work. This is to be expected given the difficulty of generating a reliable dataset of this magnitude, either experimental or computational. This problem is especially exacerbated in materials-related projects as many synthesis methods are lengthy and difficult to procure. preference towards ANNs may have been expected, given the limited number of articles, no clear trend emerges. We now present experimental [5, 6, 24] and computational [46, 47] examples: ANN [6, 47], RF [5], DT [46], and BO [6, 24].

2.3.1. Artificial Neural Network (ANN)

The crystal graph convolutional neural network (CGCNN) model can accurately learn material properties from graphical representations of atomic crystal structures, called "crystal graphs". Park and

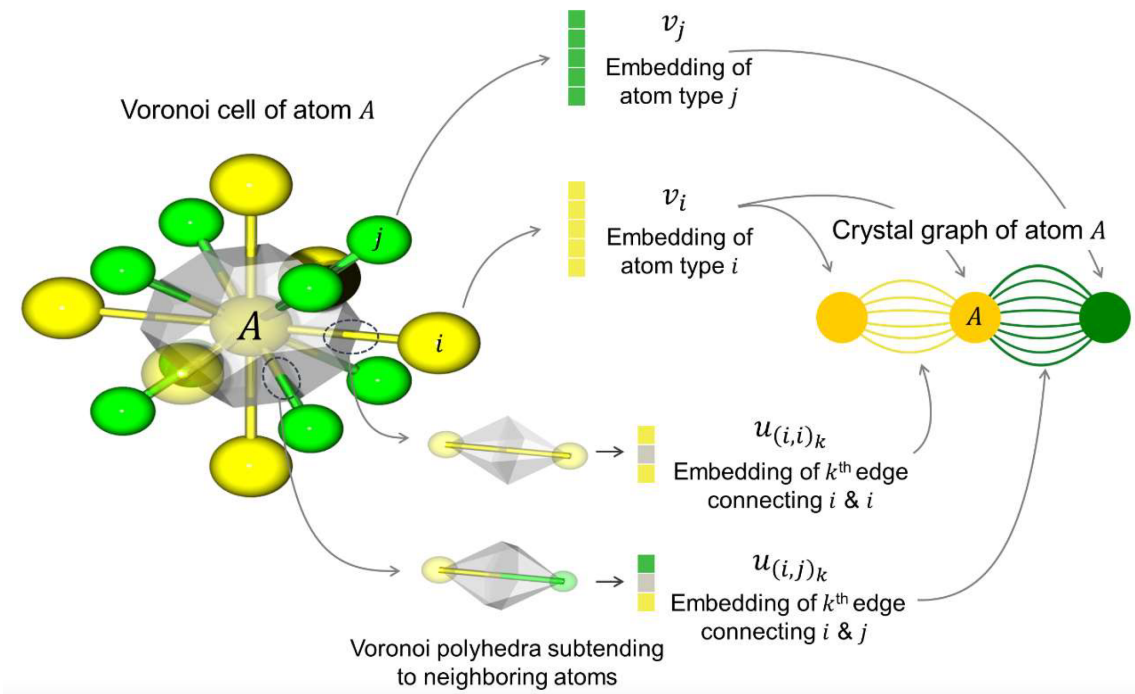

Figure 10: Visual representation of the improved crystal graph convolutional neural network (iCGCNN) crystal graph. On the left is an illustration of the Voronoi cell of Atom A, which is connected to its twelve nearest neighbors. On the right is the local environment of A. Each node and edge is embedded with vectors that contain information about the relationship between each constituent atom (v_i, v_j) and its neighbors $(\mathbf{u}_{(i,i)_k}, \mathbf{u}_{(i,j)_k})$. Additionally, edge vectors contain information (e.g. solid angle, area, and volume) about the Voronoi polyhedra. Reproduced with permission from Park, C. W.; Wolverton, C. Phys. Rev. Materials 2020, 4 (6), 063801. [47]

Wolverton [47] designed an improved framework of the CGCNN model, called improved crystal graph convolutional neural network (iCGCNN), which incorporated Voronoi tessellated crystal structures, 3-body explicit correlations of neighboring atoms, and an optimized chemical representation of interatomic bonds in the crystal graphs, all of which are absent in CGCNN (Figure 10). First, a training/testing dataset consisting of 180 000 DFT entries from the Open Quantum Materials Database [70] was created. CGCNN and iCGCNN were compared in their accuracy of predicting the thermodynamic stability of inorganic materials. Then, both models were used to conduct separate ML-assisted HiTp searches to discover new stable compounds. The new framework was shown to have 20 % higher accuracy than those of CGCNN on DFT calculated thermodynamic stability and a success rate that is 2.4 times higher than CGCNN. Using iCGCNN, they were also able to identify 97 novel stable compounds from 132 600 screened $ThCR_2Si_2$-type compounds through only 757 DFT calculations which corresponds to a success rate that is 130 times higher than that of an undirected HiTp search.

Gómez-Bombarelli et al. [6] screened 40 000 organic light-emitting diode (OLED) molecules with thermally activated delayed fluorescence (TADF) character randomly selected from a library of 1.6 million software-generated candidates using an ANN combined with BO. Then, the highest-ranking molecules based on external quantum efficiency (EQE) predicted by the ANN were promoted to time-dependent density functional theory (TD-DFT) simulation. After BO, 400 000 molecules were screened in total. Results from the TD-DFT simulation found thousands of emitters predicted to be highly efficient, with about 900 being extremely promising. The top candidates, chosen by humans, were then validated using experimental synthesis. Gómez-Bombarelli et al. [6] was able to perform an integrated high-throughput virtual screening method targeting novel TADF OLED emitters, which resulted in the discovery of new devices up to 22 % EQE, which can be applied to other areas of organic electronics.

2.3.2. Random Forest (RF)

Gaultois et al. [5] used RF to predict promising new thermoelectric materials via a user-friendly ML-based web engine. The engine suggested thermoelectric compositions based on a pre-screening of a dataset consisting of 25 000 known materials from a myriad of sources, both experimental and computational. These predictions were then experimentally validated with two new compounds. They specifically focus on a set of compounds derived from the engine, $RE_{12}Co_5Bi$ (RE = Gd, Er), which exhibited high thermoelectric performance [80]. The engine successfully predicted that this set of materials had low thermal and high electrical conductivities, but modest Seebeck coefficients, all of which were then additionally verified experimentally. The engine is the first example of ML being utilized to suggest an experimentally viable new compound from true chemical white space, with no prior characterization, that can eventually replace traditional trial-and-error techniques in the search for new materials.

2.3.3. Decision Tree (DT)

Meredig et al. [46] developed a ML model using data from over 15 000 DFT calculations to predict the thermodynamic stability of arbitrary compounds one million times faster than when just using DFT and without knowledge of crystal structure. The model was used to scan 1.6 million candidate compositions and predict 4500 new stable materials. Combining a physically motivated heuristic with a ML model and using it on a large database of quantum mechanical calculations provides a new approach for extremely rapid computational materials screening.

2.3.4. Bayesian Optimization (BO)

Sakurai et al. [24] optimized a multilayer, ultranarrow-band wavelength-selective thermal radiator using electromagnetic simulations in sets of 200 or 400 simulations in a BO/AD scheme. For computational tractability, candidates were divided into groups of approximately 200 000 each. The optimizable multilayer template consisted of 18 layers with variable total thickness (21 discrete choices) and Ge, Si, or SiO_2 as the choices for each layer. The maximum figure of merit (a function of spectral normal intensity, spectral blackbody intensity, and min/max considered wavelengths) was typically obtained within 168 000 000 calculations, comprising ∼2 % of the total possible number of structures. They identified a structure with a predicted Q-factor of 273 and experimentally validated to have a Q-factor of 188 (compare with highest reported narrow-band thermal radiator Q-factor of ∼200 according to the authors).

3. A Caution about Cross-validation (CV)

A common pitfall in materials discovery involves the use of CV. If the goal of an approach is to predict fundamentally new materials (i.e. materials extrapolation rather than interpolation), a special "grouping" CV scheme (termed G-CV in this work) may be used to ensure the model predictions are not overly optimistic. Meredig et al. [81] first introduced the idea of leave-one-cluster-out cross-validation (LOCO-CV) or G-CV and Sparks et al. [82] discussed the difficulty of making predictions when many mechanisms interact to cause outstanding properties. Sparks et al. [82] described how ML can be used for structure-composition-property-processing relationships and review successful examples of materials discovery for structural materials (fatigue, failure), high-entropy alloys, and bulk metallic glasses. For example, in the case of [22], all training data for the Co−V−Zr ternary were removed before making predictions in that group (hence G-CV). Kauwe et al. [12] performed CV on chemical formula groups rather than on all of the training data as a whole to make sure that cross-validated predictions were not simply interpolations between temperatures within a chemical formula group. To illustrate, the "trails" seen in the ML parity plots of Figure 11 exhibiting systemic deviation from parity are likely present because of the G-CV scheme. By taking a non-group CV approach, the model would likely favor temperature interpolation and mild temperature extrapolation, causing the trails to disappear at the expense of heavily overoptimistic predictive performance. We believe the question, "are my model

predictions overly optimistic?", is wise to ask when pursuing true materials discovery.

4. An Eye Towards Extraordinary Predictions

Related to the need for specialized assessment of extrapolative performance (Section 3), making extraordinary predictions can be a difficult task. Due to ambiguity of the definition of extraordinary predictions, we provide three possible definitions:

1. Experimentally or computationally validated predictions with better performance than any of the initial training dataset (also referred to as "better-than-input")

2. Experimentally or computationally validated predictions with performance on par with top performers (e.g. falls into top 1 % of the dataset as in [83])

3. Experimentally or computationally validated predictions with holistically ideal performance for a particular application including e.g. cost, toxicity, and abuse-tolerance (difficult to quantify).

From Section 2.1, we see that extraordinary predictions (definitions 1. and 2.) are commonplace due to a mixture of low number of training datapoints, simplicity of the model space (e.g. two continuous variables), and interpolative predictions. Likewise, from Section 2.2 and Section 2.3, we see that extraordinary predictions for large number of training datapoints, complex model spaces, and extrapolative (i.e. out-of-dataset) predictions are more difficult to attain. Kauwe et al. [83] analyzed the ability of ML models to predict extraordinary materials by holding out the top 1 % of compounds for a given property and training on the bottom 99 %. This was done for six different materials properties such as thermal expansion. They definitely show that extrapolation is possible, and furthermore, they show that a classification approach outperforms a regression approach. They reason that extrapolating extraordinary predictions is unlikely when the fundamental mechanism of the extraordinary prediction is different from the training dataset and that many examples of that mechanism need to be supplied. They also suggest that input data accuracy and consistency is a non-trivial issue.

In a successful example of extraordinary prediction (definition 2) [26], the top candidates from the considered ternary and quaternary inorganic solids (Figure 12) were selected for validation and confirmed to be ultraincompressible and to be superhard at low loads. Tehrani et al. [26] also discuss nuances

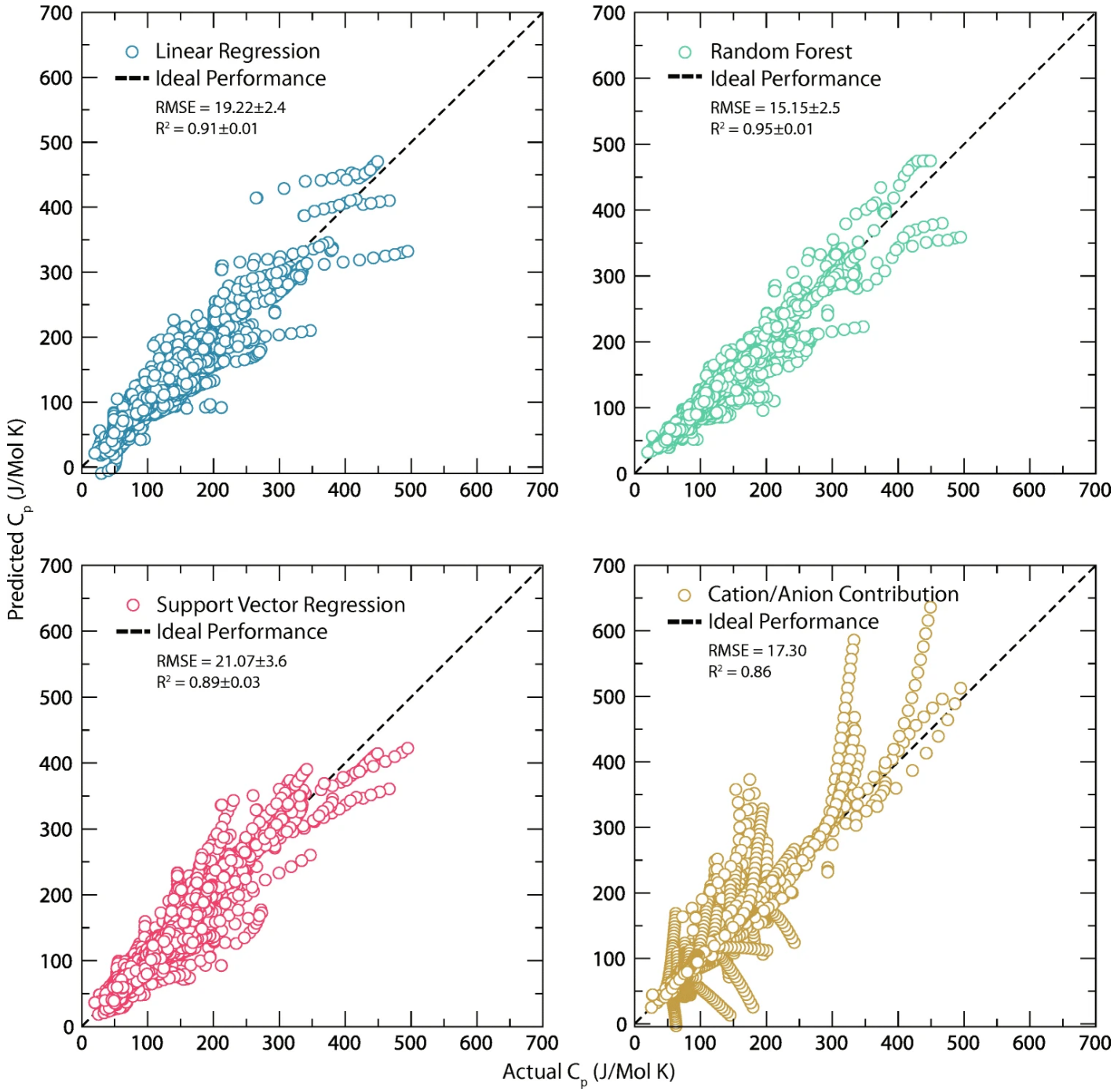

Figure 11: Grouping cross-validation (G-CV) parity plots for heat capacity predictions by linear regression (LR) (top-left), random forest (RF) (top-right), support vector machine (SVM) (bottom-left), and cation/anion contribution (CAC) (bottom-right) vs. actual heat capacity. G-CV was applied by sorting training data into chemical formula groups resulting in predictions that are extrapolations to new formulas rather than simple interpolation between temperatures of a certain chemical formula. This is likely the cause of parity "trails" (i.e. systemic bias for certain chemical formula groups) in LR, RF, and SVM methods. CAC (a legacy, non- machine learning (ML) approach) likely exhibited optimistically low root mean square error (RMSE) due to probable repeats between chemical formulae of fitted CAC coefficients (legacy work) and the G-CV data. Reproduced from Kauwe, S. K.; Graser, J.; Vazquez, A.; Sparks, T. D. Integrating Materials and Manufacturing Innovation 2018, 7 (2), 43–51[12]; licensed under a Creative Commons Attribution (CC BY) license (http://creativecommons.org/licenses/by/4.0/).

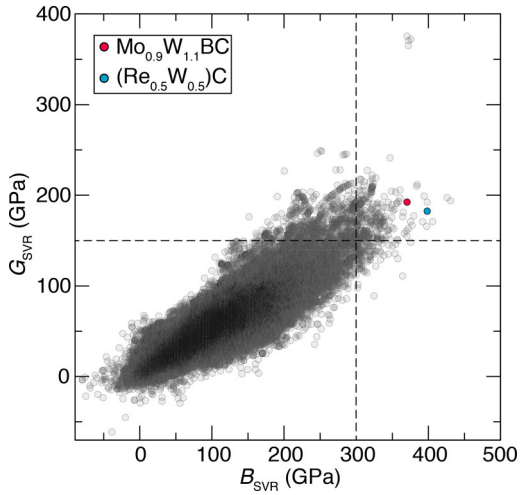

Figure 12: Predicting extraordinary ultraincompressible, superhard materials. support vector machine (SVM) predictions of bulk (B) and shear (G) moduli for 118 288 inorganic compounds. Binary candidates have already been thoroughly explored, so the top ternary ($Re_{0.5}W_{0.5}C$, blue circle) and quaternary ($Mo_{0.9}W_{1.1}BC$, red circle) candidate were each identified and selected for synthesis and characterization. Due to presence of graphite impurities in synthesized $Re_{0.5}W_{0.5}C$, $ReWC_{0.8}$ was used as an alternative. Both $ReWC_{0.8}$ and $Mo_{0.9}W_{1.1}BC$ were synthesized and confirmed as being superhard at low loads and ultraincompressible, indicating a successful example of extraordinary material discovery. Reproduced with permission from Tehrani, A. M.; Oliynyk, A. O.; Parry, M.; Rizvi, Z.; Couper, S.; Lin, F.; Miyagi, L.; Sparks, T. D.; Brgoch, J. Journal of the American Chemical Society 2018, 140 (31), 9844–9853.[26]

of measured performance such as whether hardness at low loads is a valid metric for superhardness considerations and to what extent the predicted compounds are viable for real-life applications.

For an in-depth treatment of extraordinary material predictions, see Kauwe et al. [83].

5. Conclusion

Machine learning (ML) techniques can be sorted into rough categories based on the size of the training data used for the model: 1–100, 101–10 000, and 10 000+. We demonstrate the most comprehensive set of experimentally and computationally validated examples in the literature to date and to our knowledge. Based on the distribution of techniques used in the articles, it is clear that Bayesian optimization (BO) and support vector machine (SVM) are most often used for 1–100 and 101–10 000 training dataset size ranges, respectively, whereas 10 000+ has too few examples with too much variation to establish a trend. The low number of 10 000+ validation articles relative to other size ranges illustrates the difficulty of obtaining large, high-fidelity, materials science datasets which often requires extensive curation or are simply non-existent.

We also find that adaptive design (AD) is successfully paired with BO, SVM, and other validation ML articles and that material discovery rates have been enhanced through its use. Feature selection (FS)

schemes, sometimes augmented by domain knowledge, play an important role in many validation articles. In other cases, experimental or computational high-throughput (HiTp) techniques vastly increase the amount of available homogeneous data and are even paired with AD and/or FS schemes as described earlier.

Many materials discovery articles use and benefit from grouping cross-validation (G-CV) which allows for extrapolative predictive performance to be assessed more accurately. We also find that extraordinary prediction (Section 4) is practically guaranteed for small datasets where interpolation is the primary mechanism of improved performance and much more difficult for large datasets where extrapolation is required for extraordinary material discovery.

The increase of experimentally or computationally validated articles in recent years (50 total articles in this work) and the powerful ML, FS, AD, and HiTp methods used in the articles, often in combination with each other, demonstrate that materials informatics is continuing to penetrate the materials science discipline and accelerating material discoveries for real-world applications.

Acronyms

AD adaptive design 1, 3, 25
ANN artificial neural network 2
ARES Autonomous Research System 19

BMA Bayesian model averaging 5
BO Bayesian optimization 1, 3, 23

CA correlation analysis 12
CAC cation/anion contribution 17
CGCNN crystal graph convolutional neural network 20
CIF crystallographic information file 14
CMS combinatorial magnetron sputtering 2
CNT carbon nanotube 19
COMBO COMmon Bayesian Optimization 5
CPD canonical polyadic decomposition 19
CR-FS cluster resolution feature selection 11
CRC chemically relevant composition 19
CRR capacity retention rate 18
CV cross-validation 3
CVMR cross-validated misclassification rate 10

DAC diamond anvil cell 18
DFT density functional theory 2
DoE design of experiments 5
DT decision tree 11

EA evolutionary algorithm 14
EGO efficient global optimization 10
EI expected improvement 3
EQE external quantum efficiency 20
ERT extremely randomized tree 18

FAB-HMEs factorized asymptotic Bayesian inference hierarchical mixture of experts 7
FEM finite element method 2
FS feature selection 1, 12, 25

G-CV grouping cross-validation 1, 14, 25
GA genetic algorithm 14
GBDT gradient boosting decision tree 20
GBR gradient boosting regression 18
GCMC grand canonical Monte Carlo 19
GPR Gaussian process regression 3

HEA high-entropy alloy 12
HiTp high-throughput 1, 2, 25
HOIP hybrid organic-inorganic perovskite 18

iCGCNN improved crystal graph convolutional neural network 20

KG Knowledge Gradient 10
kNN k-nearest neighbor 11
KRR kernel ridge regression 11

LASSO least absolute shrinkage and selection operator 11
LOCO-CV leave-one-cluster-out cross-validation 22
LR linear regression 10

MAE mean absolute error 5
MAECV cross-validated mean absolute error 18
MAX $M_{n+1}AX_n$ 7
MBE molecular beam epitaxy 3
ML machine learning 1, 2, 23
MOF metal-organic framework 19
MPB morphotropic phase boundary 7
MSE mean square error 10

NMF non-negative matrix factorization 19

OER oxygen evolution reaction 8
OLED organic light-emitting diode 20

PLS partial least squares 11
PLS-DA partial least-squares discriminant analysis 14
PR polynomial regression 8

RBF radial basis function 10
RF random forest 3
RFE recursive feature elimination 11
RMSE root mean square error 13, 14
RMSECV cross-validated root mean square error 17
RR ridge regression 18
RRR residual resistivity ratio 3

SMC sequential Monte Carlo 5

SMILES simplified molecular-input line-entry system 5

SMOTE synthetic minority oversampling technique 11

SR symbolic regression 3

STE spin-driven thermoelectric 7

SVD singular value decomposition 19

SVM support vector machine 1, 3, 23

TADF thermally activated delayed fluorescence 20

TD-DFT time-dependent density functional theory 20

TMR training misclassification rate 10

XRD X-ray diffraction 7

XRF X-ray fluorescence 7

References

[1] Balachandran, P. V.; Kowalski, B.; Sehirlioglu, A.; Lookman, T. Experimental Search for High-Temperature Ferroelectric Perovskites Guided by Two-Step Machine Learning. *Nature Communications* **2018**, *9*.

[2] Bucior, B. J.; Bobbitt, N. S.; Islamoglu, T.; Goswami, S.; Gopalan, A.; Yildirim, T.; Farha, O. K.; Bagheri, N.; Snurr, R. Q. Energy-Based Descriptors to Rapidly Predict Hydrogen Storage in Metal–Organic Frameworks. *Molecular Systems Design & Engineering* **2019**, *4*, 162–174.

[3] Cao, B.; Adutwum, L. A.; Oliynyk, A. O.; Luber, E. J.; Olsen, B. C.; Mar, A.; Buriak, J. M. How to Optimize Materials and Devices via Design of Experiments and Machine Learning: Demonstration Using Organic Photovoltaics. *ACS Nano* **2018**, *12*, 7434–7444.

[4] Chen, Y.; Tian, Y.; Zhou, Y.; Fang, D.; Ding, X.; Sun, J.; Xue, D. Machine Learning Assisted Multi-Objective Optimization for Materials Processing Parameters: A Case Study in Mg Alloy. *Journal of Alloys and Compounds* **2020**, *844*, 156159.

[5] Gaultois, M. W.; Oliynyk, A. O.; Mar, A.; Sparks, T. D.; Mulholland, G. J.; Meredig, B. Perspective: Web-Based Machine Learning Models for Real-Time Screening of Thermoelectric Materials Properties. *APL Materials* **2016**, *4*.

[6] Gómez-Bombarelli, R. et al. Design of Efficient Molecular Organic Light-Emitting Diodes by a High-Throughput Virtual Screening and Experimental Approach. *Nature Materials* **2016**, *15*, 1120–1127.

[7] Gzyl, A. S.; Oliynyk, A. O.; Mar, A. Half-Heusler Structures with Full-Heusler Counterparts: Machine-Learning Predictions and Experimental Validation. *Crystal Growth & Design* **2020**,

[8] Gzyl, A. S.; Oliynyk, A. O.; Adutwum, L. A.; Mar, A. Solving the Coloring Problem in Half-Heusler Structures: Machine-Learning Predictions and Experimental Validation. *Inorganic Chemistry* **2019**, *58*, 9280–9289.

[9] Homma, K.; Liu, Y.; Sumita, M.; Tamura, R.; Fushimi, N.; Iwata, J.; Tsuda, K.; Kaneta, C. Optimization of a Heterogeneous Ternary Li3PO4-Li3BO3-Li2SO4Mixture for Li-Ion Conductivity by Machine Learning. *Journal of Physical Chemistry C* **2020**, *124*, 12865–12870.

[10] Hou, Z.; Takagiwa, Y.; Shinohara, Y.; Xu, Y.; Tsuda, K. Machine-Learning-Assisted Development and Theoretical Consideration for the Al 2 Fe 3 Si 3 Thermoelectric Material. *ACS Applied Materials and Interfaces* **2019**, *11*, 11545–11554.

[11] Iwasaki, Y.; Sawada, R.; Stanev, V.; Ishida, M.; Kirihara, A.; Omori, Y.; Someya, H.; Takeuchi, I.; Saitoh, E.; Yorozu, S. Identification of Advanced Spin-Driven Thermoelectric Materials via Interpretable Machine Learning. *npj Computational Materials* **2019**, *5*, 6–11.

[12] Kauwe, S. K.; Graser, J.; Vazquez, A.; Sparks, T. D. Machine Learning Prediction of Heat Capacity for Solid Inorganics. *Integrating Materials and Manufacturing Innovation* **2018**, *7*, 43–51.

[13] Kim, K. et al. Deep-Learning-Based Inverse Design Model for Intelligent Discovery of Organic Molecules. *npj Computational Materials* **2018**, *4*, 67.

[14] Li, X.; Hou, Z.; Gao, S.; Zeng, Y.; Ao, J.; Zhou, Z.; Da, B.; Liu, W.; Sun, Y.; Zhang, Y. Efficient Optimization of the Performance of Mn2+-Doped Kesterite Solar Cell: Machine Learning Aided Synthesis of High Efficient Cu2(Mn,Zn)Sn(S,Se)4 Solar Cells. *Solar RRL* **2018**, *2*.

[15] Menon, A.; Childs, C. M.; Poczós, B.; Washburn, N. R.; Kurtis, K. E. Molecular Engineering of Superplasticizers for Metakaolin-Portland Cement Blends with Hierarchical Machine Learning. *Advanced Theory and Simulations* **2019**, *2*, 1800164.

[16] Min, K.; Choi, B.; Park, K.; Cho, E. Machine Learning Assisted Optimization of Electrochemical Properties for Ni-Rich Cathode Materials. *Scientific Reports* **2018**, *8*, 15778.

[17] Nikolaev, P.; Hooper, D.; Webber, F.; Rao, R.; Decker, K.; Krein, M.; Poleski, J.; Barto, R.; Maruyama, B. Autonomy in Materials Research: A Case Study in Carbon Nanotube Growth. *npj Computational Materials* **2016**, *2*, 16031.

[18] Oliynyk, A. O.; Adutwum, L. A.; Harynuk, J. J.; Mar, A. Classifying Crystal Structures of Binary Compounds AB through Cluster Resolution Feature Selection and Support Vector Machine Analysis. *Chemistry of Materials* **2016**, *28*, 6672–6681.

[19] Oliynyk, A. O.; Adutwum, L. A.; Rudyk, B. W.; Pisavadia, H.; Lotfi, S.; Hlukhyy, V.; Harynuk, J. J.; Mar, A.; Brgoch, J. Disentangling Structural Confusion through Machine Learning: Structure Prediction and Polymorphism of Equiatomic Ternary Phases ABC. *Journal of the American Chemical Society* **2017**, *139*, 17870–17881.

[20] Oliynyk, A. O.; Antono, E.; Sparks, T. D.; Ghadbeigi, L.; Gaultois, M. W.; Meredig, B.; Mar, A. High-Throughput Machine-Learning-Driven Synthesis of Full-Heusler Compounds. *Chemistry of Materials* **2016**, *28*.

[21] Raccuglia, P.; Elbert, K. C.; Adler, P. D.; Falk, C.; Wenny, M. B.; Mollo, A.; Zeller, M.; Friedler, S. A.; Schrier, J.; Norquist, A. J. Machine-Learning-Assisted Materials Discovery Using Failed Experiments. *Nature* **2016**, *533*, 73–76.

[22] Ren, F.; Ward, L.; Williams, T.; Laws, K. J.; Wolverton, C.; Hattrick-Simpers, J.; Mehta, A. Accelerated Discovery of Metallic Glasses through Iteration of Machine Learning and High-Throughput Experiments. *Science Advances* **2018**, *4*.

[23] Rickman, J. M.; Chan, H. M.; Harmer, M. P.; Smeltzer, J. A.; Marvel, C. J.; Roy, A.; Balasubramanian, G. Materials Informatics for the Screening of Multi-Principal Elements and High-Entropy Alloys. *Nature Communications* **2019**, *10*, 1–10.

[24] Sakurai, A.; Yada, K.; Simomura, T.; Ju, S.; Kashiwagi, M.; Okada, H.; Nagao, T.; Tsuda, K.; Shiomi, J. Ultranarrow-Band Wavelength-Selective Thermal Emission with Aperiodic Multilayered Metamaterials Designed by Bayesian Optimization. *ACS Central Science* **2019**, *5*, 319–326.

[25] Shamp, A.; Terpstra, T.; Bi, T.; Falls, Z.; Avery, P.; Zurek, E. Decomposition Products of Phosphine under Pressure: PH2 Stable and Superconducting? *Journal of the American Chemical Society* **2016**, *138*, 1884–1892.

[26] Tehrani, A. M.; Oliynyk, A. O.; Parry, M.; Rizvi, Z.; Couper, S.; Lin, F.; Miyagi, L.; Sparks, T. D.; Brgoch, J. Machine Learning Directed Search for Ultraincompressible, Superhard Materials. *Journal of the American Chemical Society* **2018**, *140*, 9844–9853.

[27] Wahab, H.; Jain, V.; Tyrrell, A. S.; Seas, M. A.; Kotthoff, L.; Johnson, P. A. Machine-Learning-Assisted Fabrication: Bayesian Optimization of Laser-Induced Graphene Patterning Using in-Situ Raman Analysis. *Carbon* **2020**, *167*, 609–619.

[28] Wakabayashi, Y. K.; Otsuka, T.; Krockenberger, Y.; Sawada, H.; Taniyasu, Y.; Yamamoto, H. Machine-Learning-Assisted Thin-Film Growth: Bayesian Optimization in Molecular Beam Epitaxy of SrRuO3 Thin Films. *APL Materials* **2019**, *7*.

[29] Weng, B.; Song, Z.; Zhu, R.; Yan, Q.; Sun, Q.; Grice, C. G.; Yan, Y.; Yin, W. J. Simple Descriptor Derived from Symbolic Regression Accelerating the Discovery of New Perovskite Catalysts. *Nature Communications* **2020**, *11*, 1–8.

[30] Wen, C.; Zhang, Y.; Wang, C.; Xue, D.; Bai, Y.; Antonov, S.; Dai, L.; Lookman, T.; Su, Y. Machine Learning Assisted Design of High Entropy Alloys with Desired Property. *Acta Materialia* **2019**, *170*, 109–117.

[31] Wu, S.; Kondo, Y.; Kakimoto, M.-a.; Yang, B.; Yamada, H.; Kuwajima, I.; Lambard, G.; Hongo, K.; Xu, Y.; Shiomi, J.; Schick, C.; Morikawa, J.; Yoshida, R. Machine-Learning-Assisted Discovery of Polymers with High Thermal Conductivity Using a Molecular Design Algorithm. *npj Computational Materials* **2019**, *5*, 66.

[32] Xue, D.; Balachandran, P. V.; Yuan, R.; Hu, T.; Qian, X.; Dougherty, E. R.; Lookman, T. Accelerated Search for BaTiO3-Based Piezoelectrics with Vertical Morphotropic Phase Boundary Using Bayesian Learning. *Proceedings of the National Academy of Sciences of the United States of America* **2016**, *113*, 13301–13306.

[33] Xue, D.; Xue, D.; Yuan, R.; Zhou, Y.; Balachandran, P. V.; Ding, X.; Sun, J.; Lookman, T. An Informatics Approach to Transformation Temperatures of NiTi-Based Shape Memory Alloys. *Acta Materialia* **2017**, *125*, 532–541.

[34] Yuan, R.; Liu, Z.; Balachandran, P. V.; Xue, D. D.; Zhou, Y.; Ding, X.; Sun, J.; Xue, D. D.; Lookman, T. Accelerated Discovery of Large Electrostrains in BaTiO3-Based Piezoelectrics Using Active Learning. *Advanced Materials* **2018**, *30*.

[35] Zhang, Z.; Mansouri Tehrani, A.; Oliynyk, A. O.; Day, B.; Brgoch, J. Finding the Next Superhard Material through Ensemble Learning. *Advanced Materials* **2020**, 2005112.

[36] Zhang, D.; Oliynyk, A. O.; Duarte, G. M.; Iyer, A. K.; Ghadbeigi, L.; Kauwe, S. K.; Sparks, T. D.; Mar, A. Not Just Par for the Course: 73 Quaternary Germanides RE4 M2 XGe4 (RE = La-Nd, Sm, Gd-Tm, Lu; M = Mn-Ni; X = Ag, Cd) and the Search for Intermetallics with Low Thermal Conductivity. *Inorganic Chemistry* **2018**, *57*, 14249–14259.

[37] Zhuo, Y.; Hariyani, S.; Armijo, E.; Abolade Lawson, Z.; Brgoch, J. Evaluating Thermal Quenching Temperature in Eu3+-Substituted Oxide Phosphors via Machine Learning. *ACS Applied Materials and Interfaces* **2020**, *12*, 5244–5250.

[38] Zhuo, Y.; Mansouri Tehrani, A.; Oliynyk, A. O.; Duke, A. C.; Brgoch, J. Identifying an Efficient, Thermally Robust Inorganic Phosphor Host via Machine Learning. *Nature Communications* **2018**, *9*.

[39] Balachandran, P. V.; Xue, D.; Theiler, J.; Hogden, J.; Lookman, T. Adaptive Strategies for Materials Design Using Uncertainties. *Scientific Reports* **2016**, *6*, 19660.

[40] Balachandran, P. V. Data-Driven Design of B20 Alloys with Targeted Magnetic Properties Guided by Machine Learning and Density Functional Theory. *Journal of Materials Research* **2020**, *35*, 890–897.

[41] Balachandran, P. V.; Young, J.; Lookman, T.; Rondinelli, J. M. Learning from Data to Design Functional Materials without Inversion Symmetry. *Nature Communications* **2017**, *8*.

[42] Balachandran, P. V.; Shearman, T.; Theiler, J.; Lookman, T. Predicting Displacements of Octahedral Cations in Ferroelectric Perovskites Using Machine Learning. *Acta Crystallographica Section B: Structural Science, Crystal Engineering and Materials* **2017**, *73*, 962–967.

[43] Ju, S.; Shiga, T.; Feng, L.; Hou, Z.; Tsuda, K.; Shiomi, J. Designing Nanostructures for Phonon Transport via Bayesian Optimization. *Physical Review X* **2017**, *7*, 021024.

[44] Lu, S.; Zhou, Q.; Ouyang, Y.; Guo, Y.; Li, Q.; Wang, J. Accelerated Discovery of Stable Lead-Free Hybrid Organic-Inorganic Perovskites via Machine Learning. *Nature Communications* **2018**, *9*, 3405.

[45] Mannodi-Kanakkithodi, A.; Pilania, G.; Huan, T. D.; Lookman, T.; Ramprasad, R. Machine Learning Strategy for Accelerated Design of Polymer Dielectrics. *Scientific Reports* **2016**, *6*, 20952.

[46] Meredig, B.; Agrawal, A.; Kirklin, S.; Saal, J. E.; Doak, J. W.; Thompson, A.; Zhang, K.; Choudhary, A.; Wolverton, C. Combinatorial Screening for New Materials in Unconstrained Composition Space with Machine Learning. *Physical Review B* **2014**, *89*, 094104.

[47] Park, C. W.; Wolverton, C. Developing an Improved Crystal Graph Convolutional Neural Network Framework for Accelerated Materials Discovery. *Physical Review Materials* **2020**, *4*, 063801.

[48] Seko, A.; Hayashi, H.; Kashima, H.; Tanaka, I. Matrix- and Tensor-Based Recommender Systems for the Discovery of Currently Unknown Inorganic Compounds. *Physical Review Materials* **2018**, *2*, 013805.

[49] Sendek, A. D.; Yang, Q.; Cubuk, E. D.; Duerloo, K. A. N.; Cui, Y.; Reed, E. J. Holistic Computational Structure Screening of More than 12 000 Candidates for Solid Lithium-Ion Conductor Materials. *Energy and Environmental Science* **2017**, *10*, 306–320.

[50] Talapatra, A.; Boluki, S.; Duong, T.; Qian, X.; Dougherty, E.; Arróyave, R. Autonomous Efficient Experiment Design for Materials Discovery with Bayesian Model Averaging. *Physical Review Materials* **2018**, *2*.

[51] Meredig, B. Five High-Impact Research Areas in Machine Learning for Materials Science. *Chemistry of Materials* **2019**, *31*, 9579–9581.

[52] Murdock, R. J.; Kauwe, S. K.; Wang, A. Y.-T.; Sparks, T. D. Is Domain Knowledge Necessary for Machine Learning Materials Properties? *ChemRxiv* **2020**, 8.

[53] Wang, A. Y.-T.; Murdock, R. J.; Kauwe, S. K.; Oliynyk, A. O.; Gurlo, A.; Brgoch, J.; Persson, K. A.; Sparks, T. D. Machine Learning for Materials Scientists: An Introductory Guide toward Best Practices. *Chem. Mater.* **2020**, 12.

[54] Paszke, A. et al. In *Advances in Neural Information Processing Systems 32*; Wallach, H., Larochelle, H., Beygelzimer, A., dAlché-Buc, F., Fox, E., Garnett, R., Eds.; Curran Associates, Inc., 2019; pp 8024–8035.

[55] Pedregosa, F. et al. Scikit-Learn: Machine Learning in Python. *Journal of Machine Learning Research* **2011**, *12*, 2825–2830.

[56] Ueno, T.; Rhone, T. D.; Hou, Z.; Mizoguchi, T.; Tsuda, K. COMBO: An Efficient Bayesian Optimization Library for Materials Science. *Materials Discovery* **2016**, *4*, 18–21.

[57] Ong, S. P. Python Materials Genomics (Pymatgen): A Robust, Open-Source Python Library for Materials Analysis. *Computational Materials Science* **2013**, 6.

[58] Ward, L.; Agrawal, A.; Choudhary, A.; Wolverton, C. A General-Purpose Machine Learning Framework for Predicting Properties of Inorganic Materials. *npj Computational Materials* **2016**,

[59] Choudhary, K. et al. The Joint Automated Repository for Various Integrated Simulations (JARVIS) for Data-Driven Materials Design. *npj Computational Materials* **2020**, *6*, 173.

[60] The MathWorks, I. Statistics and Machine Learning Toolbox. 2020.

[61] The MathWorks, I. Deep Learning Toolbox. 2020.

[62] Kuhn, M. Building Predictive Models in r Using the Caret Package. *Journal of Statistical Software, Articles* **2008**, *28*, 1–26.

[63] Meyer, D.; Dimitriadou, E.; Hornik, K.; Weingessel, A.; Leisch, F.; Chang, C.-C.; Lin, C.-C. E1071: Misc Functions of the Department of Statistics, Probability Theory Group. 2020.

[64] Venables, W. N.; Ripley, B. D. *Modern Applied Statistics with s*, 4th ed.; Springer: New York, 2002.

[65] Butler, K. T.; Davies, D. W.; Cartwright, H.; Isayev, O.; Walsh, A. Machine Learning for Molecular and Materials Science. *Nature* **2018**, *559*, 547–555.

[66] Gaultois, M. W.; Sparks, T. D.; Borg, C. K.; Seshadri, R.; Bonificio, W. D.; Clarke, D. R. Data-Driven Review of Thermoelectric Materials: Performance and Resource Onsiderations. *Chemistry of Materials* **2013**, *25*, 2911–2920.

[67] Hoar, B. B.; Lu, S.; Liu, C. Machine-Learning-Enabled Exploration of Morphology Influence on Wire-Array Electrodes for Electrochemical Nitrogen Fixation. *Journal of Physical Chemistry Letters* **2020**, *11*, 4625–4630.

[68] Yan, B.; Gao, R.; Liu, P.; Zhang, P.; Cheng, L. Optimization of Thermal Conductivity of UO2–Mo Composite with Continuous Mo Channel Based on Finite Element Method and Machine Learning. *International Journal of Heat and Mass Transfer* **2020**, *159*, 120067.

[69] Jain, A.; Ong, S. P.; Hautier, G.; Chen, W.; Richards, W. D.; Dacek, S.; Cholia, S.; Gunter, D.; Skinner, D.; Ceder, G.; a. Persson, K. The Materials Project: A Materials Genome Approach to Accelerating Materials Innovation. *APL Materials* **2013**, *1*, 011002.

[70] Kirklin, S.; Saal, J. E.; Meredig, B.; Thompson, A.; Doak, J. W.; Aykol, M.; Rühl, S.; Wolverton, C. The Open Quantum Materials Database (OQMD): Assessing the Accuracy of DFT Formation Energies. *npj Computational Materials* **2015**, *1*, 15010.

[71] Villars, P.; Cenzual, K. Pearson's Crystal Data: Crystal Structure Database for Inorganic Compounds. 2014.

[72] Ward, L. et al. Matminer: An Open Source Toolkit for Materials Data Mining. *Computational Materials Science* **2018**, *152*, 60–69.

[73] Oliynyk, A. O.; Buriak, J. M. Virtual Issue on Machine-Learning Discoveries in Materials Science. *Chemistry of Materials* **2019**, *31*, 8243–8247.

[74] Saal, J. E.; Oliynyk, A. O.; Meredig, B. Machine Learning in Materials Discovery: Confirmed Predictions and Their Underlying Approaches. *Annual Review of Materials Research* **2020**, *50*, 49–69.

[75] Bera, C.; Jacob, S.; Opahle, I.; Gunda, N. S. H.; Chmielowski, R.; Dennler, G.; Madsen, G. K. H. Integrated Computational Materials Discovery of Silver Doped Tin Sulfide as a Thermoelectric Material. *Phys. Chem. Chem. Phys.* **2014**, *16*, 19894–19899.

[76] Ghosh, N.; Harimkar, S. In *Advances in Science and Technology of Mn+1axn Phases*; Low, I., Ed.; Woodhead Publishing, 2012; pp 47–80.

[77] Tummers, B.; van der Laan, J.; Huyser, K. DataThief III Software. 2015.

[78] *MathWorks Help Center Documentation: Dummy Variables*; 2020.

[79] Jones, D. R.; Schonlau, M. Efficient Global Optimization of Expensive Black-Box Functions. *Journal of Global Optimization* **1998**, 38.

[80] Oliynyk, A. O.; Sparks, T. D.; Gaultois, M. W.; Ghadbeigi, L.; Mar, A. $Gd_{12}Co_{5.3}Bi$ and $Gd_{12}Co_{5}Bi$, Crystalline Doppelgänger with Low Thermal Conductivities. *Inorganic Chemistry* **2016**, *55*, 6625–6633.

[81] Meredig, B.; Antono, E.; Church, C.; Hutchinson, M.; Ling, J.; Paradiso, S.; Blaiszik, B.; Foster, I.; Gibbons, B.; Hattrick-Simpers, J.; Mehta, A.; Ward, L. Can Machine Learning Identify the next High-Temperature Superconductor? Examining Extrapolation Performance for Materials Discovery. *Molecular Systems Design & Engineering* **2018**, *3*, 819–825.

[82] Sparks, T. D.; Kauwe, S. K.; Parry, M. E.; Tehrani, A. M.; Brgoch, J. Machine Learning for Structural Materials. *Annual Review of Materials Research* **2020**, *50*, 27–48.

[83] Kauwe, S. K.; Graser, J.; Murdock, R.; Sparks, T. D. Can Machine Learning Find Extraordinary Materials? *Computational Materials Science* **2020**, *174*.